Materials Today Bio 16 (2022) 100368

Contents lists available at ScienceDirect

Materials Today Bio

journal homepage: www.journals.elsevier.com/materials-today-bio

Advances in the development of biodegradable coronary stents: A translational perspective

Jiabin Zong [a], Quanwei He [a], Yuxiao Liu [a], Min Qiu [a], Jiehong Wu [a,*], Bo Hu [a,**]

[a] Department of Neurology, Union Hospital, Tongji Medical College, Huazhong University of Science and Technology, Wuhan, 430022, China

ARTICLE INFO

Keywords:
Cardiovascular scaffolds
Translational research
In-stent restenosis
Bioresorbable stents
Stent optimization

ABSTRACT

Implantation of cardiovascular stents is an important therapeutic method to treat coronary artery diseases. Bare-metal and drug-eluting stents show promising clinical outcomes, however, their permanent presence may create complications. In recent years, numerous preclinical and clinical trials have evaluated the properties of bioresorbable stents, including polymer and magnesium-based stents. Three-dimensional (3D) printed-shape-memory polymeric materials enable the self-deployment of stents and provide a novel approach for individualized treatment. Novel bioresorbable metallic stents such as iron- and zinc-based stents have also been investigated and refined. However, the development of novel bioresorbable stents accompanied by clinical translation remains time-consuming and challenging. This review comprehensively summarizes the development of bioresorbable stents based on their preclinical/clinical trials and highlights translational research as well as novel technologies for stents (e.g., bioresorbable electronic stents integrated with biosensors). These findings are expected to inspire the design of novel stents and optimization approaches to improve the efficacy of treatments for cardiovascular diseases.

1. Introduction

Coronary artery diseases (CADs) are the primary cause of mortality and morbidity with increasing incidences worldwide, thus imposing a substantial socioeconomic burden [1]. Minimally invasive cardiovascular stents can be implanted into impaired vessels to provide mechanical support to the blood vessel wall—substantially improving revascularization's quality [2]. The application of a bare-metal stent (BMS) in clinical practice has improved the efficacy of percutaneous coronary intervention (PCI) [3,4]. However, BMS implantation results in different adverse events, including in-stent restenosis (ISR) and stent thrombosis (ST) [5]. The implantation of a drug-eluting stent (DES) dramatically reduces the ISR rate. However, the delayed vascular re-endothelialization caused by the non-selective nature of drugs in the stents results in increased incidences of late stent thrombosis (LST) and very late stent thrombosis (VLST) [6–9]. Moreover, prolonged dual anti-platelet therapy

Abbreviations: Ag, silver; Ag^{+}, silver ions; AMS, absorbable metal stent; Au, gold; BDMS, biodegradable metallic stent; BDPS, biodegradable polymeric stent; BMS, bare-metal stent; BNL, base neo-intimal length; BRS, bioresorbable stent; Cl, chloride; Cl^{-}, chloride ions; CS, chitosan; Cu, copper; CADs, coronary artery diseases; DAPT, dual anti-platelet therapy; DES, drug-eluting stent; DREAMS, drug-eluting absorbable metal scaffold; EC, endothelial cell; ECAP, equal-channel angular pressure; EDM, energy dispersive spectroscopy; EEM, external elastic membrane; EL, elongation to fracture; Fe, iron; Fe^{2+}, ferrous ions; Fe–O, iron oxide; GO, graphene oxide; H^{+}, hydrogen ions; HA, hyaluronic acid; HUVECs, human umbilical vein endothelial cells; ISR, in-stent restenosis; IVUS, intravascular ultrasonography; JDBM, JiaoDa BioMg; LDH, layered double-hydroxide; LLL, late lumen loss; LOI, lumen occlusion index; LST, late stent thrombosis; MACE, major adverse cardiac event; MAO, micro-arc oxidation; Mg, magnesium; Mg^{2+}, magnesium ions; MgF_2, magnesium fluoride; MgO, magnesium oxide; micro-CT, micro-computerized tomography; Mn, manganese; MPS, metal-polymer composite stent; MRI, magnetic resonance imaging; N, nitrogen; NA, neo-intimal area; OCT, optical coherence tomography; OH^{-}, hydroxyl radicals; P, phosphorus; PCI, percutaneous coronary intervention; PCL, polycaprolactone; Pd, palladium; PDA, polydopamine; PDLLA, poly-D,L-lactic acid; PGDA, poly(glycerol-dodecanoate) acrylate; PIIID, plasma immersion ion implantation and deposition; PLA, polylactic acid; PLGA, poly-lactic-co-glycolide; PLLA, poly-L-lactide acid; PM, powder metallurgy; Pt, platinum; PTA, percutaneous transluminal angioplasty; SEM, scanning electron microscopy; SES, sirolimus-eluting stent; SMMs, shape-memory materials; SMPs, shape-memory polymers; ST, stent thrombosis; STEMI, ST-segment-elevation myocardial infarction; Ta, tantalum; T_g, glass transition temperature; TiO_2, titanium dioxide; TLF, target lesion failure; TLR, target lesion revascularization; UTS, ultimate tensile strength; VGs, vein grafts; VSMCs, vascular smooth muscle cells; WLT, wire lumen thickness; YS, yield strength; Zn, zinc; Zn^{2+}, zinc ions.

* Corresponding author.
** Corresponding author.
E-mail addresses: wujiehong@mail.hust.edu.cn (J. Wu), hubo@mail.hust.edu.cn (B. Hu).

https://doi.org/10.1016/j.mtbio.2022.100368
Received 29 March 2022; Received in revised form 25 June 2022; Accepted 13 July 2022
Available online 19 July 2022

(DAPT) after the implantation of a DES increases the risk of bleeding [7]. These shortcomings of non-degradable scaffolds have encouraged the development of a bioresorbable stent (BRS) [10]. The main features of BMS, DES, and BRS are listed in Table 1. BRS provides temporary mechanical support to prevent acute elastic recoil until vascular remodeling and functional recovery [10]. After implantation into the vessels, its gradual degradation contributes to the restoration of vascular systolic function and reduces the risk of LST [11,12]. A schematic diagram of vascular responses to BMS, DES, and BRS *in vivo* is presented in Fig. 1. BRS comprises biodegradable polymeric stent (BDPS) and biodegradable metallic stent (BDMS) [13].

Table 1
The main features of 3 main types of stents–BMS, DES and BRS.

	BMS	DES	BRS
Mechanical stress	permanent	permanent	temporary
Tensile strength	high	high	high (metallic stents) low (polymeric stents)
Coatings	none	possessed	possessed
Risk of thrombosis	low	late	transient
In-stent restenosis	high	low	moderate
Inflammation	low	moderate/high	high
Vessel size mismatch	none	none	possible

Preclinical studies, especially *in vivo* assays are critical for evaluating the properties of BRS, including its mechanical strength, biodegradation behavior, and biocompatibility. In recent times, some novel methods have been developed to evaluate stent properties *in vivo*. For example, semi-quantitative optical coherence tomography (OCT) imaging can be used to measure *in vivo* biodegradation behavior of BRS [14,15]. Additionally, animal models have aided better evaluation of stent performance; e.g., the New Zealand rabbit iliac artery model has been utilized to assess endothelial cell (EC) function restoration [16]. These preclinical

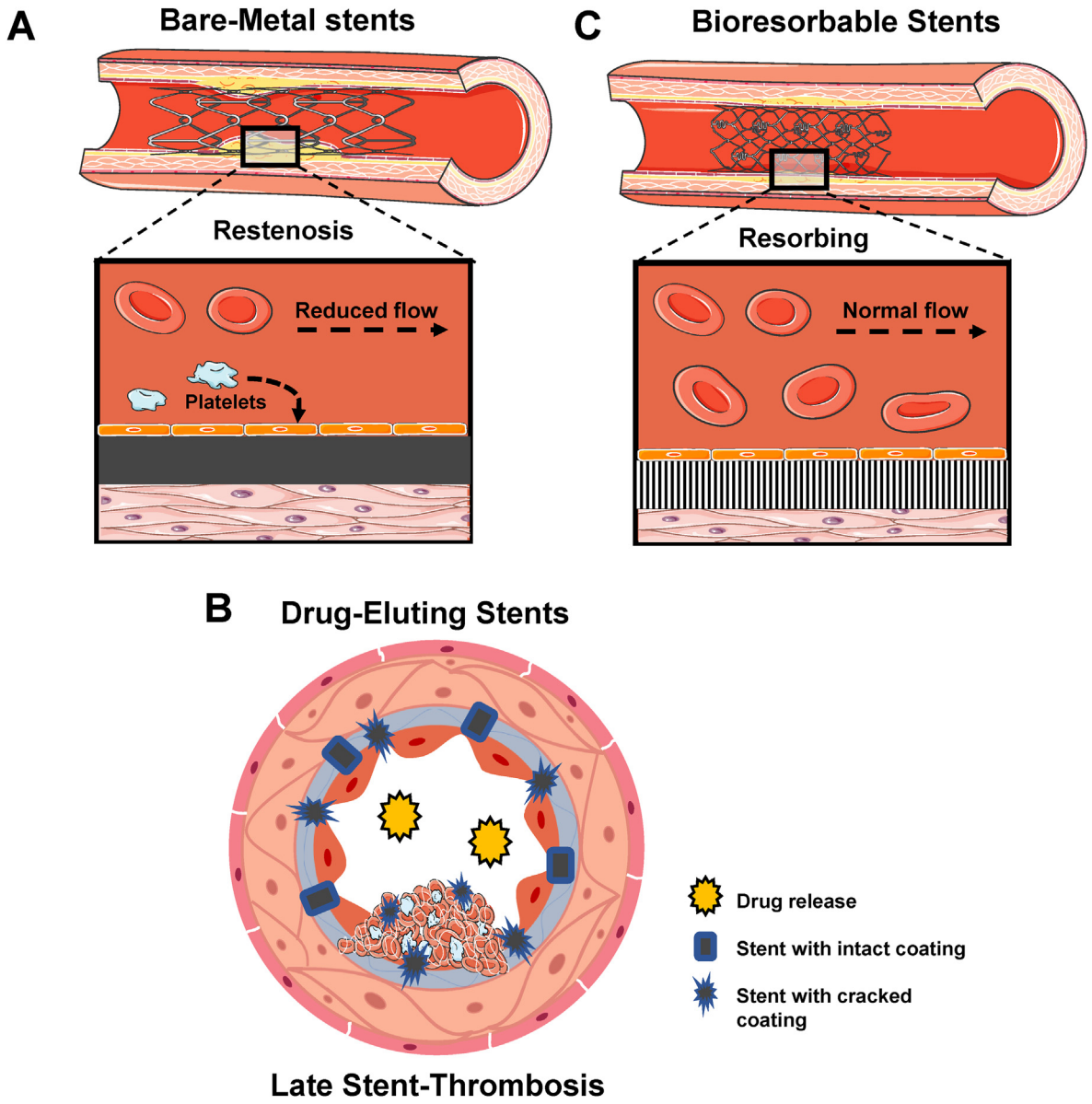

Fig. 1. Schematic diagram of vascular responses of BMS, DES and BRS *in vivo*. A) The initial stent: bare-metal stent (BMS). These stents possess great mechanical strength and can be fabricated to have reduced thickness. However, the robust mechanical support also causes neo-intimal hyperplasia. B) The second generation of stent: drug-eluting stent (DES). The eluting drug was an anti-mitotic agent, inhibiting the proliferation of SMCs. However, impaired endothelial regeneration and vasomotion occur, increasing the risk of late stent thrombosis (ST). C) Bioresorbable stent (BRS). These stents are resorbed over 6 months to 2 years, alleviating long-term chronic inflammation and enabling endothelial regeneration. Reproduced with permission [214]. Copyright 2020, John Wiley and Sons.

Table 2
Summary of clinical trials of BDPS.

Device	Stent design	Trial	Results	Refs
Igaki–Tamai	Material: PLLA; Coating: None; Drug: None	Follow up 50 patients with 84 Igaki–Tamai for >10 years	ST: 4%; 1 subacute and 1 very late thrombosis; Survival rates for all-cause death 87%, for cardiac death 98%, for MACE[a] 50%; TLR[b]:16% (1 year), 22% (5 years), and 38% (10 years)	[39]
Absorb BVS 1.0	Material: PLLA; Coating: PDLLA[c]; Drug: Everolimus	ABSORB Cohort A: Follow up 30 patients with single de novo lesions treated with 30 BVS for 5 years	ST: 0; LLL[d]: 0.44 ± 0.35 mm; MACE: 3.3%	[33]
Absorb BVS 1.1	Material: PLLA; Coating: PDLLA; Drug: Everolimus	Absorb B1/B2: Follow up 101 patients for 2/3 years	ST:0; LLL: 0.27 ± 0.32 mm; MACE: 6.9%	[40, 41]
Absorb BVS 1.1	Material: PLLA; Coating: PDLLA; Drug: Everolimus	Absorb Extend: Follow up 512 patients for 1 year	ST: 0.8%; TLF[e]: 4.9%; MACE: 4.3%	[42]
Absorb BVS 1.1	Material: PLLA; Coating: PDLLA; Drug: Everolimus	Absorb III: Follow up 1322 patients for 5 years	ST: 1.5%; TLF: 7.8%	[43]
Absorb BVS 1.1	Material: PLLA; Coating: PDLLA; Drug: Everolimus	AIDA: Follow up 895 patients for 2 years	ST: 3.5%; TLF: 11.7%	[44]
DeSolve	Material: PLLA; Coating: PLLA; Drug: Novolimus	DESolve Nx: Follow up 126 patients in a multi-center trial for 2 years	ST: 0.8%; TLF: 5.7%; MACE: 5.7%	[45]
Fortitude	Material: PLLA; Coating: None; Drug: Sirolimus	FORTITUDE Study: Follow up 63 patients with single de novo coronary artery lesions for 9 months	ST: 0; TLF: 3.3%; MACE: 4.9%; Narrowing in the mean area: 9.1%	[46]
Xinsorb	Material: PLLA; Coating: PDLLA; Drug: Sirolimus	Follow up 30 patients with single de novo coronary artery lesions for 6 months	ST: 0; LLL: 0.18 ± 0.21 mm; MACE: 0	[47]
Ideal BioStent	Material: Polylactide anhydride; Coating: Salicylate; Drug: Sirolimus	WHISPER-trial: Follow up to 11 patients	High neointimal growth	[48]
ART18Z	Material: PDLLA; Coating: None; Drug: None	ARTDIVA-trial: Follow up 30 patients with single de novo lesions for 6 months	TLR: 10%; MACE: 0; Angiographic recoil: 4.3%; In-stent diameter stenosis: 12 ± 7%	[42]
REVA	Material: PTD-PC[f]; Coating: None; Drug: None	RESORB: Follow up 27 patients for 6 months	TLR: 66.7%; LLL: 1.81 mm; Leading to the scaffold redesign	[42]
ReZolve	Material: PTD-PC; Coating: None; Drug: Sirolimus	RESTORE-study: Follow up 50 patients for 1 year	Acute recoil: 3.8 ± 6.7%; LLL: 0.29 ± 0.33 mm at 12 months; MACE: 16.7% at 6 months	[42]
ReZolve2	Material: PTD-PC; Coating: None; Drug: Sirolimus	RESTORE-II: Follow up 125 patients	Ongoing	[49]

[a] MACE, major adverse cardiac event.
[b] TLR, target lesion revascularization.
[c] PDLLA, poly-D,L-lactic acid.
[d] LLL, late lumen loss.
[e] TLF, target lesion failure.
[f] PTD-PC, poly-tyrosine-derived polycarbonate.

trials are crucial for clinical translation; the design of clinical trials should be based on the results of *in vivo* and *in vitro* experiments. Moreover, basic experiments shed new insights into stent optimization. Clinical trials for various BRS types have shown differential clinical efficacies, limitations, and optimization direction. Lessons learned from clinical trials also prompt the development of next-generation stents. Current optimization strategies mainly include developing novel stent platforms, functionalizing stent coatings, and adopting more precise engineering technologies [17].

Novel technologies for BRS also provide new insights into the development of cardiovascular scaffolds. For example, the bioresorbable electronic stents containing biosensors can convey information about the internal status of stents in real time [18–22]. 3D printing technologies enable designing BRS, which is specifically tailored to each patient for better clinical outcomes [21,23–25].

In this review, we summarize the properties, modification strategies, and future challenges to different stent types. Novel technologies applied in BRS are also discussed in detail. Additionally, this review focuses on the results of the preclinical and clinical trials for vascular stents and their potential clinical impact. These findings are expected to inspire new avenues for evaluating novel stent materials, assessment methods, and optimization approaches to improve the efficacy of treatment for CADs.

2. Biodegradable polymeric stent

2.1. Properties of BDPS

The mechanical properties of the vascular stent need to reach benchmark values: elongation to fracture (EL) > 15–18%, ultimate tensile strength (UTS) > 300 MPa and yield strength (YS) > 200 MPa [26–28]. Generally, bioresorbable polymers could not provide sufficient radial strength for vascular remodeling [29]. In addition, some polymers with acceptable mechanical strength recoiled immediately after implantation, with harmful or even fatal consequences [30]. Therefore, the BDPS should be designed with self-expandability to avoid acute recoil; however, this also increases the stent size limiting their use in small vessel diseases [31]. Polymers will eventually degrade into water and carbon dioxide by hydrolysis of ester bonds [32,33]. Studies found that the degradation rate of BDPS can be regulated by molecular weight, composition, glass transition temperature (T_g), and morphology of the polymer materials [34].

The BDPS possesses good biocompatibility as giant cells and leukocytes could remove their degradation debris, thus avoiding severe chronic inflammatory response [35]. For instance, histological analyses of BDPS in animal experiments showed reduced inflammatory responses

[36]. However, some studies also showed that polymers may have a cytotoxic effect on macrophages [37]. Furthermore, BDPS lacks radiopacity [38]. Nevertheless, BDPS could be visualized by CT or MRI with a radio-opaque marker located on stents [18]. The clinical trials to evaluate the properties of BDPS are summarized in Table 2 [33,39–49].

2.2. Optimization and future challenges of BDPS

The main challenge remains to improve the radial strength of BDPS. Several approaches have been proven effective to strengthen BDPS, including manufacturing techniques, optimizing geometric parameters, and improving scaffold thickness [50]. High molecular weight polymers could increase the entanglement and length of covalently-bonded molecular chains, which can improve the strain-to-break and wear resistance of the BDPS [51]. Improving the crystallinity of semi-crystalline polymers could increase the stiffness and heat or chemical resistance of BDPS [52]. Transforming the molecular structure by controlling the interior structure of the polymer chain orientation can also improve the mechanical strength of BDPS [53]. Meanwhile, modifying geometric parameters is another method to improve the radial strength of BDPS. For example, the Igaki–Tamai stent has a thick strut in the shape of a zig-zag helical coil, thus having a high vessel coverage [54]. The biodegradable, non-toxic lignocellulosic fiber from renewable resources (e.g., wood) has been investigated as a potential reinforcing component for biodegradable polymers as this kind of fiber confers great strength and is more economical than traditional synthetic fibers [18,55–57]. In addition, fabricating BDPS with a carbon dioxide laser or adopting a new slide–and–lock mechanism has been proven to improve the mechanical properties of BDPS [58]. The shape-memory PCLAU incorporating Fe_3O_4 nanoparticles can provide sufficient strength for stent implantation [59]. The biocompatibility of BDPS can be improved by plasma surface treatment and adopting high molecular weight poly-L-lactide acid (PLLA) [54]. Furthermore, altering the crystallinity, molecular weight, and hydrophilicity of the polymers could improve the degradation behavior of the BDPS [60–62].

Future studies are required to investigate optimization methods to make next-generation BDPS qualified as a novel treatment strategy for CADs. For example, BDPS should have a thin strut thickness but with sufficient radial strength [18]. In addition, the degradation rate should match the vascular remodeling time to avoid late lumen loss (LLL) or target lesion revascularization (TLR) [18].

2.3. Self-expandable stents based on shape-memory polymers

2.3.1. Biodegradable shape-memory polymeric stents

Owing to their behavioral versatility, shape-memory materials (SMMs), which are smart materials, maybe the key to advancements in the next-generation stents [21]. The shape transformation can be triggered by diverse stimuli, such as heating above the transition temperature (Tg), electric/magnetic fields, light, etc. [63]. This shape-memory behavior contributes to the reduction in conduit size for delivery, and allows self-expansion without assisting devices [24,64]. Biodegradable shape-memory polymers (SMPs), in particular, are highly suited for self-expandable stents owing to their high recoverable strain (up to 400%), controllability of recovery behavior, flexibility, minimal toxicity, lightweight, ease of processing, and low-price [65,66]. SMP-BRS can be inserted into the impaired vessels through minimally invasive surgery in folded or contraction state. Triggered by *in vivo* or external stimuli, SMPs can recover to their desired original shapes at the target site, thus achieving full self-expansion rapidly to impede the stent migration [65]. Common SMPs employed in BRS include polycaprolactone (PCL), polylactic acid (PLA) and lactide-based copolymers (e.g., PLLA) [67,68].

Despite the potential of SMPs for designing biodegradable self-expandable stents, its clinical translation remains challenging. Venkataraman et al. developed a biodegradable bi-layered stent based on PLLA and poly-lactic-co-glycolide (PLGA), which can fully self-expand at about 37 °C in approximately 8 min in an aqueous environment [69]. Although the time for full expansion significantly decreases to a few minutes, the ideal self-expansion time should be less than 1 min to avoid stent migration and favor *in vivo* deployment. Additionally, the gradual loss of mechanical forces and stent blockade caused by bacterial colonization may lead to serious complications after the implantation of SMP stents [69,70]. Duarah et al. have developed a rapid self-expandable stent using a bio-based hyperbranched polyurethane/carbon dot-silver (HPU/C-D-Ag) nanocomposite [70]. An added biocompatible nanomaterial interacted with SMPs, thus facilitating faster self-expansion. The HPU/CD-Ag nanocomposite achieved self-expansion (>99%) at (37 ± 1) °C within only 20 s, suggesting a significant decrease. Carbon dots are added at the smallest scale to improve the mechanical properties of stents. Silver nanoparticles (AgNP), an effective infection-resistant material, can be used to inhibit biofilm formation to avoid stent blockage caused by bacterial colonization, thus reducing the incidence of complications. The biological assessment shows that HPU/CD-Ag nanocomposite inhibits the growth of *Staphylococcus aureus* MTCC 3160 and *Escherichia coli* MTCC 40 bacterial strains, and prevents the adherence of *Pseudomonas aeruginosa* MTCC 1688 bacterial strain to the fabricated nanocomposites [70]. Biswas et al. have synthesized a polyurethane nanohybrid for BRS applications [51]. The reduced crystallinity in the nanohybrid caused by strong dipolar interactions between polymer chains and nano-clay significantly improves flexibility and toughness. Additionally, the reduced stacking pattern of the hard segment of nanohybrid results in a significant improvement in shape memory behavior (91% recovery) at 37 °C [51]. Taken together, employing fabricated nanohybrids to develop rapid self-expandable BDPS may provide novel insights into augmenting the expandability and improving the mechanical properties of current BRS. SMP stents exhibit great potential as a novel solution to overcome the limitations of the current BRS types.

2.3.2. Advances in 3D printing of SMP stents

Using traditional fabrication methods (e.g., electrospinning, spin-coating, and molding) to construct SMP stents limit their adaptivity. The emergence of 3D printing (i.e., additive manufacturing) brings in a new era in the development of SMP stents [71]. Using the 3D printing technology, SMPs can be fabricated into individualized self-expanding stents with more complex geometries, high accuracy, and reproducibility [72]. 3D printing provides an effective and rapid prototyping method to produce customized stents, which can be tailored specifically for the patient, thus limiting the stent migration [23,24]. This personalized production of BRS provides a solution to problems previously encountered for BRS (e.g., inappropriate stent size) [23]. This individualized treatment modality may significantly improve clinical outcomes as 3D-printed BRSs are tailored to individual patient needs, especially in those with complicated lesions requiring specific stent geometries [73]. Moreover, 3D-printed stents possess other properties, including loading of specific drug substances, controlled release over time, and dose flexibility, thereby fulfilling the patients' individual clinical needs [74,75]. Additionally, 3D printing also simplifies the manufacturing for BRS. Stent structures can be directly fabricated instead of laser cutting of mini-tubes [23]. This can lead to substantial savings of raw materials and production time and resources, along with provision for improved geometrical flexibility [23].

3D printing technologies can also help investigate some unsolved problems. Yin et al. implanted a 3D-printed poly-l-actide vascular stent (PLS) into the abdominal aortas of SD rats to further study the turning point of degradation, vascular responses, and pathophysiological processes of blood vessels [76], whereby six-month was a key time point owing to the following reasons: (1) during the first 6 months, the degradation rate was slow and neointima with good barrier function was achieved; (2) after 6 months, rapid degradation occurred accompanied by reduced inflammation and intimal hyperplasia. Inspired by this promising result, the "two-stage degradation" model of 3D-printed PLS

may improve neointima function and vascular remodeling [76]. Combining 3D-printed PLS with sequential drug release and effective targeting may yield better clinical outcomes, and this warrants further clinical research.

T_g of the 3D-printed SMP stents (e.g., <20 °C or >37 °C) are not ideal for their implantation [25]. Thus, fixing the temporary shape and returning to the original shape between 20 °C and 37 °C remains challenging. Zhang et al. have developed 3D printing for a novel SMP, poly(glycerol-dodecanoate) acrylate (PGDA) to address this challenge [77]. PGDA exhibits excellent shape-memory behavior, including large fixity (100% at 20 °C) and recovery ratio (98% at 37 °C), high cycling stability (>100 times), and rapid recovery time (0.4 s at 37 °C) [25]. Thus, with the suitable Tg in the range of 20–37 °C, 3D-printed stents based on PGDA can be programmed at normal temperature, thus automatically accomplishing shape recovery within the human body. This greatly simplifies implantation and reduces the incidence of scald or frostbite to vessels. Additionally, *in vitro* stenting shows substantial mechanical and geometrical adaptivity for 3D-printed stents. The Young's moduli of PGDA (3.2 MPa at 37 °C) are comparable to that of vessels, thus decreasing the mechanical mismatch between targeted vessels and 3D-printed stents after implantation. The suitable rheological properties of PGDA allow for the printing of multifunctional 3D structures, especially overhanging and tilted structures [25]. Taken together, this novel 3D-printed SMP stent based on PGDA has immense potential to tackle current challenges to 3D-printing technologies, paving a new route to design personalized shape-memory stents. Further *in vivo* tests to detect long-term efficiency, safety, and degradation behavior of PGDA stents are warranted.

Significant medical advancements have been made in the application of 3D-printing technology to SMP stents. The 3D-printed personalized stents are in line with the evidence-based personalized medicine concept, which may be the future of interventional cardiology. However, it is a long way from 3D printing to the marketed clinical stent. For instance, insufficient printer resolution limits the fabrication of thinner stents. The thickness of stents affects artery coverage, blood flow, and the stent crimping. Additionally, it is difficult to achieve homogeneity and smoothness in layer-wise stent printing [24]. Therefore, more studies are needed to tackle these challenges. Additionally, examining novel printable polymers is also important. Novel materials like photo-crosslinked biobased resins possess high mechanical integrity, biocompatibility, and low viscosity grades, thereby allowing high print resolution (<10 μm) [23]. While extensive studies are required to verify their degradation and biocompatibility *in vivo*, with improvements in printer resolution and printing performance, 3D printing can produce sophisticated and smaller structures with intricate features for next-generation SMP stents.

3. Biodegradable metallic stents

3.1. Magnesium-based stents

3.1.1. Properties of Mg-based stents

Mg is a trace but essential element in the human body and therefore safe for stent implantation [78]. Studies have shown that the release of negligible magnesium ions (Mg^{2+}) during stent degradation may inhibit abnormal nerve excitation and reduce the risk of atherosclerosis [79]. Researchers implanted Mg-based stents into pig coronaries to evaluate their safety. These *in vivo* studies indicated that Mg-based stents possess great biocompatibility [80]. Mg-based stents have thin strut thickness, high mechanical strength, and high elastic modulus [81]. However, they are prone to fracture due to their low plastic deformation and high brittleness [82].

In vitro experiments demonstrated that Mg degraded readily in aqueous solutions and unstable magnesium oxide (MgO) would form upon exposure to air [83]. In addition, chloride ions (Cl^-) in body fluids accelerate the degradation process of Mg [83]. An *in vivo* corrosion assay showed that Mg completely degraded within 1–3 months, thus the degradation rate of Mg-based stents was too rapid for stent application [84]. The rapid degradation rate will result in premature loss of radial support, increasing the risk of arterial recoil [85]. Moreover, the uneven degradation behavior of Mg-based stents will also result in cracking and collapsing of Mg-based stents, which are associated with a high incidence of ISR [86]. The uncontrollable degradation of Mg could also lead to the excessive release of hydrogen ions (H^+), inhibiting endothelium restoration [87].

3.1.2. Clinical trials of Mg-based stents

Bosiers et al. and Peeters et al. reported promising results in a preclinical trial of absorbable metal stent (AMS) [88,89]. This attracted great attention due to the perfect procedural success rate and limb salvage rate of AMS. However, the ISR of AMS was still high [88]. AMS INSIGHT trial by Bosiers et al. compared the therapeutic effects of AMS and percutaneous transluminal angioplasty (PTA) on the treatment for critical limb ischemia (CLI) [90]. The results showed that LLL caused by intimal hyperplasia was higher in AMS group [90]. Moreover, the study also indicated that the stent recoil caused by the rapid degradation rate and insufficient radial strength may lead to AMS restenosis [90].

Erbel et al. published the results of PROGRESS AMS [91]. Partial degradation of AMS at 4 months contributed to the functional restoration of vessels. However, at 4 months, obvious restenosis could be observed because of neo-intimal hyperplasia and a reduction in the volume of the external elastic membrane (EEM). The volume reduction of EEM could be due to stent recoil and lack of mechanical integrity, indicating that next-generation Mg-based stents should be developed to have improved radial strength and moderate degradation rates. In addition, target lesion failure (TLF) and MACE at 12-months follow-up were not optimal, suggesting that a drug-eluting coating may be beneficial for AMS to achieve better clinical outcomes. Waksman et al. continued to follow up with eight patients from PROGRESS AMS for 28 months [39]. The results showed that new cases of stent recoil or neo-intimal hyperplasia were not observed [39]. Interestingly, LLL and ISR improved from 4 months to 28 months, which may be attributed to positive vessel remodeling in the late stage of AMS implantation due to complete stent degradation [39].

A drug-eluting absorbable metal scaffold (DREAMS) was developed to have improved strut geometry and better degradation behavior [92]. The BIOSOLVE-1 clinical trial evaluated the performance of the DREAMS [93]. At 6 months, significant restenosis occurred, which could be due to the reduced cross-sectional area in DREAMS. Neo-intimal hyperplasia was alleviated due to the paclitaxel-eluting coating, thus contributing less to ISR compared to the AMS. Intravascular ultrasonography (IVUS) showed that lumen loss could be attributed to neo-intimal hyperplasia and an increased extra-stent plaque area until 6 months. While from 6 to 12 months, the vessel area remained unchanged, which indicated that no negative remodeling, chronic recoil, or neo-intimal hyperplasia occurred. Besides, as the stent degraded, ISR also improved, and the TLF rate for the DREAMS significantly decreased at late time points [93]. The same team further followed up to 3 years and the results showed that LLL improved at the late time points and no additional TLFs occurred [94]. Taken together, for DREAMS, the TLF rate was promising while LLL at 6 months was not optimal [93], suggesting the need for further development of DREAMS to prevent the neo-intimal formation and acute stent recoil at the early stage after stent implantation.

DREAMS 2G, a second-generation DREAMS was developed to possess a higher radial force, higher bending flexibility, and a stronger and more flexible scaffold backbone [95]. Moreover, sirolimus-eluting PLLA polymer coating could inhibit neo-intimal hyperplasia more effectively. The BIOSOLVE-2 clinical trial evaluated the properties of DREAMS 2G [95]. Restenosis occurred at 6 months, which could be due to late scaffold recoil and neo-intimal hyperplasia [95]. However, the LLL for DREAMS 2G improved, mainly because of less neo-intimal formation compared to DREAMS 1G. At 12-months follow-up, the angiographic and clinical outcomes of DREAMS 2G were sustained [96]. In addition, Garcia et al. revealed the restoration of vasomotion and vascular geometry by

Table 3
Clinical trials of Mg-based stents.

Device	Stent design	Trial	Clinical outcomes	Refs
AMS	Coating: None; Drug: None	Preliminary study for AMS INSIGHT: 3-months follow up of 20 patients with CLI received AMS in infrapopliteal arteries	Stenosis rate: 10.5% at 1 month and 31.6% at 3 months; Limb Salvage Rate: 100%	[88]
AMS	Coating: None; Drug: None	Preliminary study for AMS INSIGHT: up to 12 months	Significant restenosis in 3 patients after 85, 107, and 181 days respectively; Limb Salvage Rate: 95%	[89]
AMS	Coating: None; Drug: None	AMS INSIGHT: Follow up 74 patients with CLI received AMS in infrapopliteal arteries and 75 patients with CLI after PTA for 6 months	Binary restenosis rate: 68.2% in AMS group and 42% in PTA group; LLL: 0.4 ± 0.8[a] mm in AMS group and 0.7 ± 0.7 mm in PTA group; Limb Salvage Rate: 97% in AMS group and 96% in PTA group	[90]
AMS	Coating: None; Drug: None	PROGRESS AMS: Follow up 63 patients with lesions of 50–99% stenosis for 12 months	ST: 0; LLL: 1.08 ± 0.49 mm at 4 months; TLF: 23.8% at 4 months and 27% at 12 months; ISR: 47.5% at 4 months	[91]
AMS	Coating: None; Drug: None	Follow up 8 patients from PROGRESS AMS up to 28 months	ST: 0; LLL: 0.1 (−0.4 to 0.9)[b] mm; In-stent diameter stenosis: 24.5% (11%–44%)	[39]
DREAMS (Biotronik)	Coating: PLGA; Drug: Paclitaxel	BIOSOLVE-I: Follow up 46 patients with lesions of 50–99% stenosis for 12 months	ST: 0; LLL: 0.65 ± 0.50 mm at 6 months and 0.52 ± 0.39 mm at 12 months; TLF: 4% at 6 months and 7% at 12 months; Lumen area stenosis: 43.38% at 6 months and 46.10% at 12 months; Neointimal hyperplasia area: 0.30 ± 0.41 mm^2 at 6 months and 0.40 ± 0.32 mm^2 at 12 months	[93]
DREAMS	Coating: PLGA; Drug: Paclitaxel	BIOSOLVE-1: 3-years follow up	ST: 0; LLL: 0.51 ± 0.46 mm at 12 months to 0.32 ± 0.32 mm at 28 ± 4 months(n = 7); TLF: no additional TLFs at 3-years follow up	[94]
DREAMS 2G (Biotronik)	Coating: PLLA; Drug: Sirolimus	BIOSOLVE-2: Follow up 123 patients with 50–99% stenosis for 6 months	ST: 0; LLL: 0.44 ± 0.36 mm; TLF: 3.3%; Neointimal hyperplasia area: 0.08 ± 0.09 mm^2; Diameter stenosis in stent: 22.6 ± 12.9 mm	[95]
DREAMS 2G	Coating: PLLA; Drug: Sirolimus	BIOSOLVE-2: 12-months follow up	ST: 0; LLL: 0.37 ± 0.25 mm at 6 months to 0.39 ± 0.27 mm at 12 months (n = 42); TLF: no additional TLFs at 12-months follow up; Diameter stenosis in stent: 19.6 ± 8.4 mm at 6 months to 20.4 ± 8.6 mm at 12 months(n = 42)	[96]
DREAMS 2G	Coating: PLLA; Drug: Sirolimus	BIOSOLVE-2: In vivo serial invasive imaging of DREAMS 2G up to 12-months	OCT results: Mean lumen area: 6.34 ± 1.86 mm^2 at 6 months (n = 65) and 6.46 ± 1.72 mm^2 at 12 months (n = 25); Minimum lumen area: 4.53 ± 1.69 mm^2 at 6 months (n = 65) and 4.81 ± 1.48 mm^2 at 12 months (n = 25); IVUS results: 6.57 ± 1.40 mm^2 at 6 months and 6.45 ± 1.28 mm^2 at 12 months	[97]
DREAMS 2G	Coating: PLLA; Drug: Sirolimus	BIOSOLVE-2: 3-years follow up	ST: 0; LLL: 0.39 ± 0.27 mm at 12 months to 0.54 ± 0.38 mm at 36 months; TLF: 6.8% at 36 months; Diameter stenosis: 3.8 ± 10.1% at 12 months and 4.1 ± 10.2% at 36 months (n = 25, angiographic)	[98]
Magmaris (Biotronik)	Coating: PLLA; Drug: Sirolimus	BIOSOLVE-3: Follow up 61 patients with lesions of 50–99% stenosis for 12 months	ST: 0; LLL: 0.39 ± 0.39 mm; TLF: 3.3% at 6 and 12 months	[99]
Magmaris	Coating: PLLA; Drug: Sirolimus	BIOSOLVE-3: 24-months follow up	ST: 0; TLF: 5.9% at 24 months	[100]
Magmaris	Coating: PLLA; Drug: Sirolimus	Preliminary study for MAGSTEMI: Follow up 20 patients with STEMI for 59–326 days	TLF: 5% at 102 days	[103]
Magmaris	Coating: PLLA; Drug: Sirolimus	MAGSTEMI: Follow up 74 patients treated with Magmaris and 76 patients treated with Orsiro for 12 months	In stent acute gain: 2.30 ± 0.48 mm (Magmaris) and 2.49 ± 0.48 mm (Orsiro); LLL: 0.61 ± 0.55 mm (Magmaris) and 0.06 ± 0.21 mm (Orsiro); In stent diameter stenosis rate: 30.3 ± 19.7% (Magmaris) and 7.7 ± 7.2% (Orsiro)	[104]
Magmaris	Coating: PLLA; Drug: Sirolimus	BIOSOLVE-4: First cohort of 1075 patients with 1121 lesions	ST: 0.5% at 6 months and 12 months; TLF: 2.7% at 6 months and 4.3% at 12 months	[105]
Magmaris	Coating: PLLA; Drug: Sirolimus	BIOSOLVE-4: Second cohort of 2054 with simple lesions	Still in progress	[106]

[a] Values are mean ± SD.
[b] Values are median (range).

assessing several serial invasive imaging methods such as IVUS [97]. Haude et al. followed up with 25 patients for 36 months and found that the TLF and LLL slightly increased from 1 to 3 years [98].

The DREAMS 2G was remarketed as "Magmaris", whereas the following BIOSOLVE-3 clinical trial evaluated the clinical performance and safety of Magmaris [99]. At 12 months, the LLL was close to that in the BIOSOLVE-2 trial and the TLF rate was acceptable [99]. No ST occurred and TLF slightly improved from 12 to 24 months [100]. Pooled results of the BIOSOLVE-2 and -3 trials indicated that the implantation of DREAMS 2G (i.e., Magmaris) could be a promising treatment strategy for CADs [100–102].

The MAGSTEMI clinical trial was initiated to further evaluate the performance of Magmaris for the treatment of ST (i.e., S-wave/T-wave)-segment-elevation myocardial infarction (STEMI) relative to the permanent metallic sirolimus-eluting stent (SES) [103,104]. In this trial, Magmaris exhibited a higher vasomotor response to drugs but resulted in a higher LLL, ISR, and TLF rate at 12-months follow-up compared to the SES [104]. Therefore, Magmaris should be further developed with an increased radial strength.

The ongoing BIOSOLVE-4 clinical trial aims to evaluate the post-market performance of Magmaris. The first cohort of 1075 patients has achieved a promising TLF rate, suggesting great clinical performance [105]. The second cohort is ongoing [106]. Clinical trials of Mg-based stents are presented in Table 3.

3.1.3. Optimization of Mg-based stents

Scientists have been trying to improve the properties of Mg-based stents by exploring novel alloys, surface modifications and coatings, and improving manufacturing strategies. Alloying can increase the mechanical strength, plasticity, and corrosion resistance of Mg-based stents [107,108]. Some alloying elements have been proven to improve the degradation behavior of Mg-based alloys, such as zinc (Zn), aluminum, manganese (Mn), calcium (Ca), lithium, strontium, and tin [109–111]. Many Mg alloys with better degradation behavior have been designed including the Mg alloy AE21, AZ31, AZ91, WE43, LAE442, ZE21B, and JiaoDa BioMg (JDBM) [112,113]. It should be noted that the JDBM, comprising of Mg–neodymium[Nd]–Zn–zirconium[Zr] alloys, exhibited significant *in vivo* biocompatibility, long-term mechanical durability,

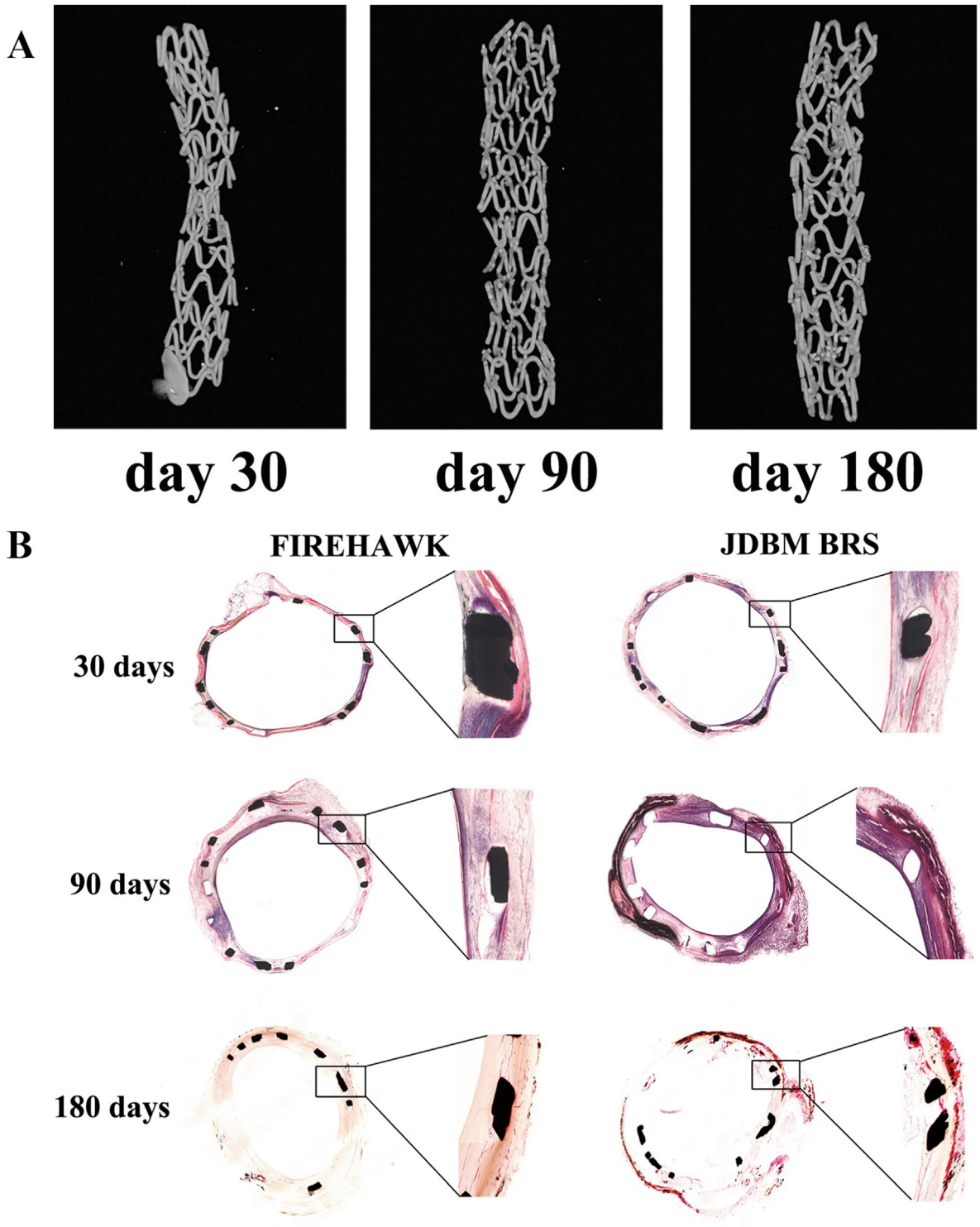

Fig. 2. Performance of JDBM stent. A) Micro-CT results of JDBM stents at 30, 90, and 180 days after implantation. JDBM stent maintained good integrity at 30 days. At 90 days, the JDBM stent still maintained the main structure. Some of the stents transferred to degradation products shown as the light gray part in the image. At 180 days, the JDBM stent degraded more intensely but maintained mechanical integrity. B) Histological images of JDBM stent and FIREHAWK stent at 30, 90, and 180 days after implantation into porcine arteries. No obvious intimal hyperplasia, thrombosis, restenosis, or intimal hyperplasia occurred in either of the stents up to 180 days. Reproduced under terms of the CC-BY license [115]. Copyright 2021, Zhu et al., published by [Nature Research].

homogeneous nano-phasic degradation patterns, and low biodegradation rate [114]. The micro-computerized tomography (micro-CT) results of residual JDBM BRS are shown in Fig. 2A. A recent study by Zhu et al. showed that the JDBM stents could provide support for vessels during the period before degradation and after implantation [115]. The JDBM began to lose its radial strength gradually with vascular physiologic reconstruction at ~6 months. In addition, *in vivo* safety and efficacy of the JDBM stent were evaluated in porcine arteries. The results showed that the vessels implanted with the JDBM stent and FIREHAWK rapamycin-eluting stent both receive complete re-endothelialization after 30 days (Fig. 2B) [115]. Moreover, there was no significant difference in the luminal area, neo-intimal area (NA) and thickness, the

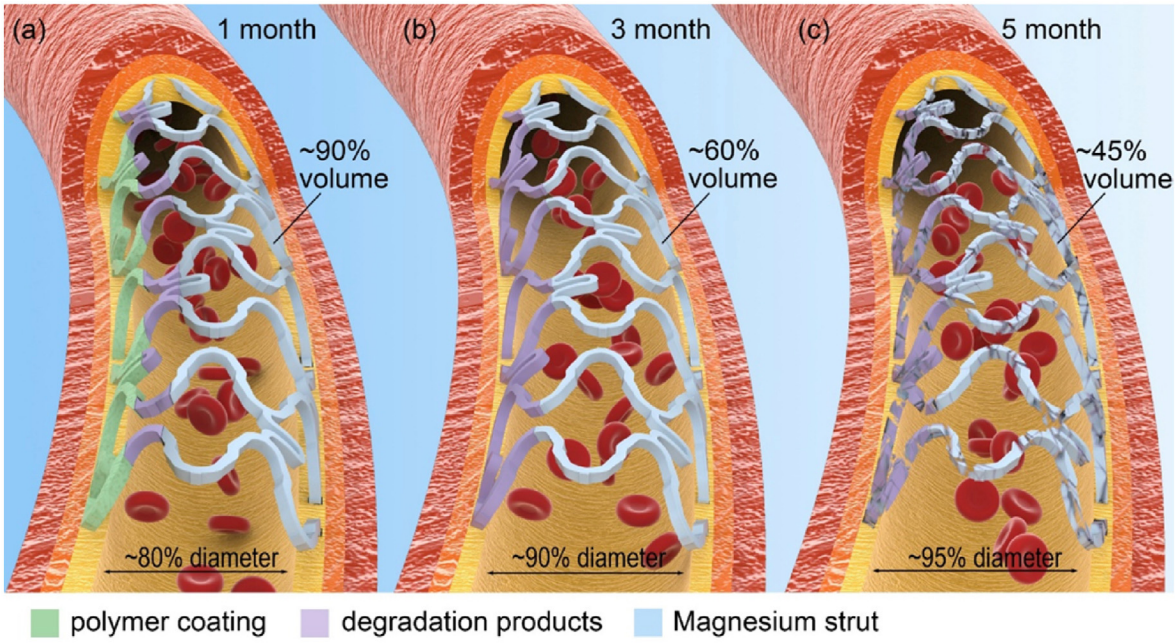

Fig. 3. Schematic diagram of the degradation process of a polymer coated Mg-based stent. The left part of the stent stands for the surface layer and right part the internal strut. After 1 month, Mg-based stent degraded under the cover of polymer coating. The major structures of the stent were still maintained while polymer coating lost integrity at 3-months follow up. After 5 months, constraint on vasomotion was removed and vasoreactivity was restored with stent eroding itself. Reproduced with permission [120]. Copyright 2019, Elsevier.

internal elastic membrane area, as well as percent stenotic lumen between the two groups [115].

Novel manufacturing strategies to achieve grain refinement can also improve the mechanical properties and degradation behavior of Mg-based stents. For example, AZ31 possesses a lower degradation rate through grain refinement produced by mechanical processing [116]. Small-sized ZM21 has higher mechanical strength [117]. In addition, 3D printing technologies, especially selective laser melting could process Mg alloys for optimized machine architectures and better corrosion control [118,119].

Surface modification, such as micro-arc oxidation (MAO), phosphating treatment, electrodeposition, and alkaline heat treatment can modify the surface chemistry and the metallurgical microstructure of Mg-based stents, improving the degradation behavior of Mg stents [120]. The schematic diagram of the degradation process of a polymer coated Mg-based stent is presented in Fig. 3. In addition, coatings can also improve the degradation behavior of Mg-based stents. Several coatings have proven effective to slow down the degradation rate of Mg-based stents (Fig. 4B).

Through technologies like the solvothermal method, atomic layer deposition, and plasma electrolytic oxidation, metal oxide coatings such as MgO and titanium dioxide (TiO_2) can be fabricated on Mg-based stents to improve the degradation behavior. TiO_2 coating has been widely used to modify Mg-based stents due to its rapid re-endothelialization, antithrombosis effect, good corrosion resistance, and great biocompatibility [121]. MgO-coating can also improve the degradation behavior of Mg-based stents [122]. However, MAO coating may affect the activity of vascular cells and its porous microstructures may weaken the protective effect on Mg stents [123]. Layered double-hydroxide (LDH) coating could promote EC adhesion, proliferation, and migration. An *in vivo* experiment showed that LDH efficiently decreased the degradation rate, indicating the anti-corrosion performance of LDH coating [124]. However, due to the poor abrasion resistance of LDH, its microstructure was easy to exfoliate and enter into circulation [125]. Inorganic non-metallic coatings such as phosphate, magnesium fluoride (MgF_2), and graphene oxide (GO) coatings possess good biocompatibility and can decrease the corrosion rate of Mg-based stents [126]. Polymer coatings, such as PLA, PLGA, PCL, hyaluronic acid (HA), polydopamine (PDA), and chitosan (CS) are promising alternatives due to their good corrosion resistance and biocompatibility [127]. Furthermore, natural polymer coatings possess better biocompatibility as well as other biological functions such as anti-bacterial and anti-thrombotic properties (Fig. 4A) [128].

As opposed to a single layer, multilayer coatings can combine the advantages of every single-layer coating to simultaneously meet the clinical stent application requirement such as good functional properties and strong bonding strength. Composite coatings may resolve the deficient bioactivity and poor adhesion of Mg-based stents. These coatings include inorganic layer/inorganic layers like MAO-LDH coating, inorganic layer/organic layers such as MgF2/PLLA and MAO/CS, organic layers/organic layers like PDA/PCL and Mg–OH-PDA-HA, and organic layers/functional biomolecular layers like the LDH/PDA/Hep hybrid [129–131]. Furthermore, the conjugation of biomolecules with hybrid coatings may boost the rapid re-endothelialization and tailor the degradation behaviors of Mg-based stents [132]. However, a systematic long-term evaluation needs to be done due to the complex degradation behaviors of the composite coatings. In addition, Mg-based metallic glasses have the potential for application as implantable materials due to their high strength, good biodegradability, large elasticity, and low elastic modulus [133,134].

3.2. Fe-based stents

3.2.1. Properties of Fe-based stents

Iron (Fe) possesses appropriate elastic modulus, radial support strength, and ductility [135]. In addition, the great formability of Fe also makes Fe-based stents easier to forge into thinner structures and special shapes like foils or foams [136]. As an indispensable element of the human body, Fe has great biocompatibility [137]. Fe will not lead to excessive release of H^+ and thus a dramatic increase of pH—therefore, Fe results in fewer alterations to the local micro-environment [138]. Studies have shown that the release of Fe from stents is negligible compared to the Fe overload concentration of blood (447 mg L^{-1})—thus, Fe will not lead to systemic toxicity. Furthermore, studies suggested that ferrous ions (Fe^{2+}) may prevent the proliferation and migration of human vascular

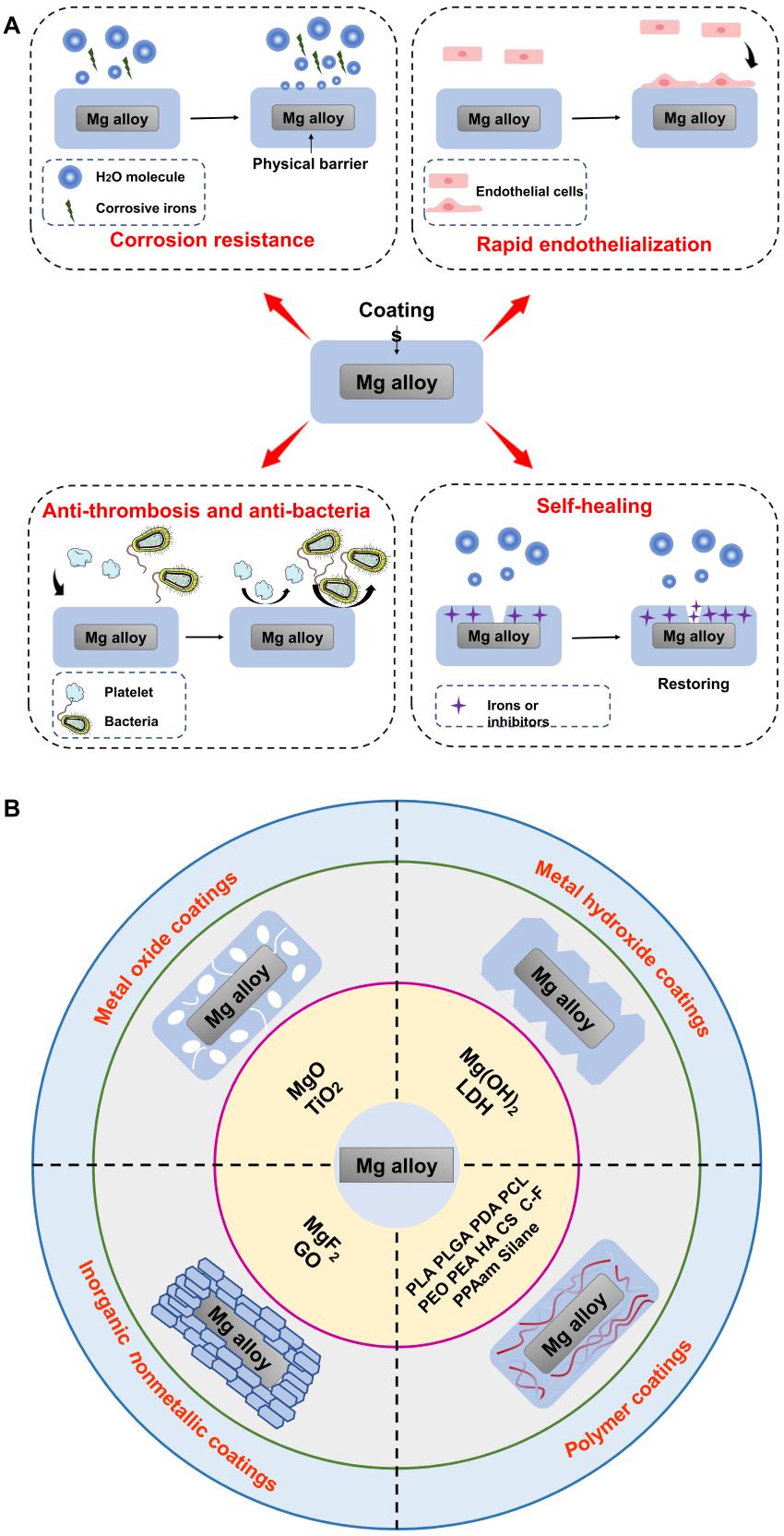

Fig. 4. Surface modification of Mg-based stents through functional coatings. A) Coatings improve the corrosion behavior and possess rapid re-endothelialization, anti-thrombosis, anti-bacteria, and self-healing effects. B) Different coatings applied to improve the properties of Mg stents, including metal oxide coatings, metal hydroxide coatings, inorganic nonmetallic coatings, and polymer coatings.

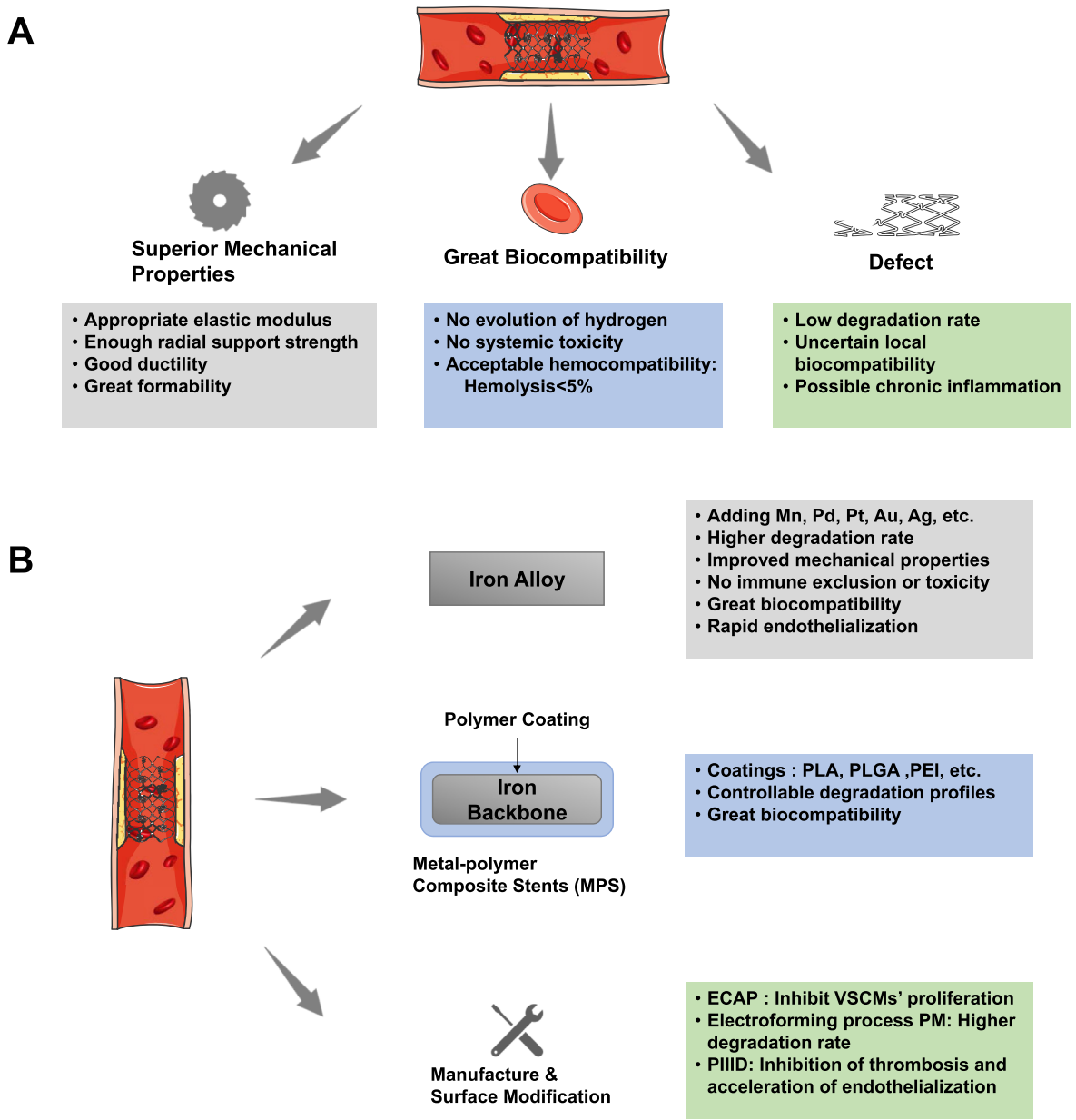

Fig. 5. Iron-based bioresorbable metallic stents. A) The properties of iron-based stents: superior mechanical properties, great biocompatibility, but low degradation rate. B) The main optimization methods to improve the properties of iron-based stents: alloying, adding polymer coatings, and surface modification. ECAP, equal channel angular pressure; PM, powder metallurgy; PIIID, plasma immersion ion implantation, and deposition.

smooth muscle cells (VSMCs) [139,140]. A hemolysis assay of Fe-based stents showed that few platelets adhered to the stent, whereas the hemolysis rate was below 5%, indicating that Fe-based stents possess great hemocompatibility [141].

The degradation rate of Fe-based stents was too slow [142]. The prolonged degradation period of Fe-based stents will lead to the accumulation of corrosion products [137]. The firm corrosion products (mainly iron oxide [Fe–O]) are retained in the encapsulating neo-intima, inhibiting vascular tissue regeneration [143]. Besides, the ferromagnetic behavior of Fe is not examinable with magnetic resonance imaging (MRI) [144]. In addition, the local biocompatibility of Fe is still controversial [145]. The direct interaction between vascular cells and Fe can produce injurious radicals during corrosion [146], such as hydroxyl radicals (OH^-), alkoxyl (RO^-), thiyl ($RS^\bullet$), thiyl peroxyl ($RSOO^\bullet$), and peroxyl ($ROO^\bullet$) radicals [147]. These highly reactive free radicals can lead to a state of oxidative stress and a series of injurious systemic events like ischemia, inflammation, and neurodegeneration by promoting oxidation and modification of nucleic acids and proteins [148].

Moreover, studies have proven that Fe-laden macrophages occurred from rarefied individual cells to clusters at the interfaces of implants [149]. Macrophages are mainly responsible for removing Fe^{2+} and Fe^{3+} from the corroding implants [150]. In addition, Fe-laden macrophages were also present in the para-aortic lymph nodes, indicating that chronic inflammation occurred after Fe-based stent implantation [151].

3.2.2. *Optimization and future challenges of Fe-based stents*

In recent years, several approaches have been shown to improve the degradation behavior of Fe-based stents without sacrificing their superior mechanical properties. These methods include alloying, coating, as well as manufacturing modifications of the interface morphology and the structure of Fe-based stents (Fig. 5) [145].

Alloying is a common process to optimize the properties of Fe-based stents [152]. To increase the degradation rate of Fe alloys, the additives should have lower electrochemical potential or be nobler than iron

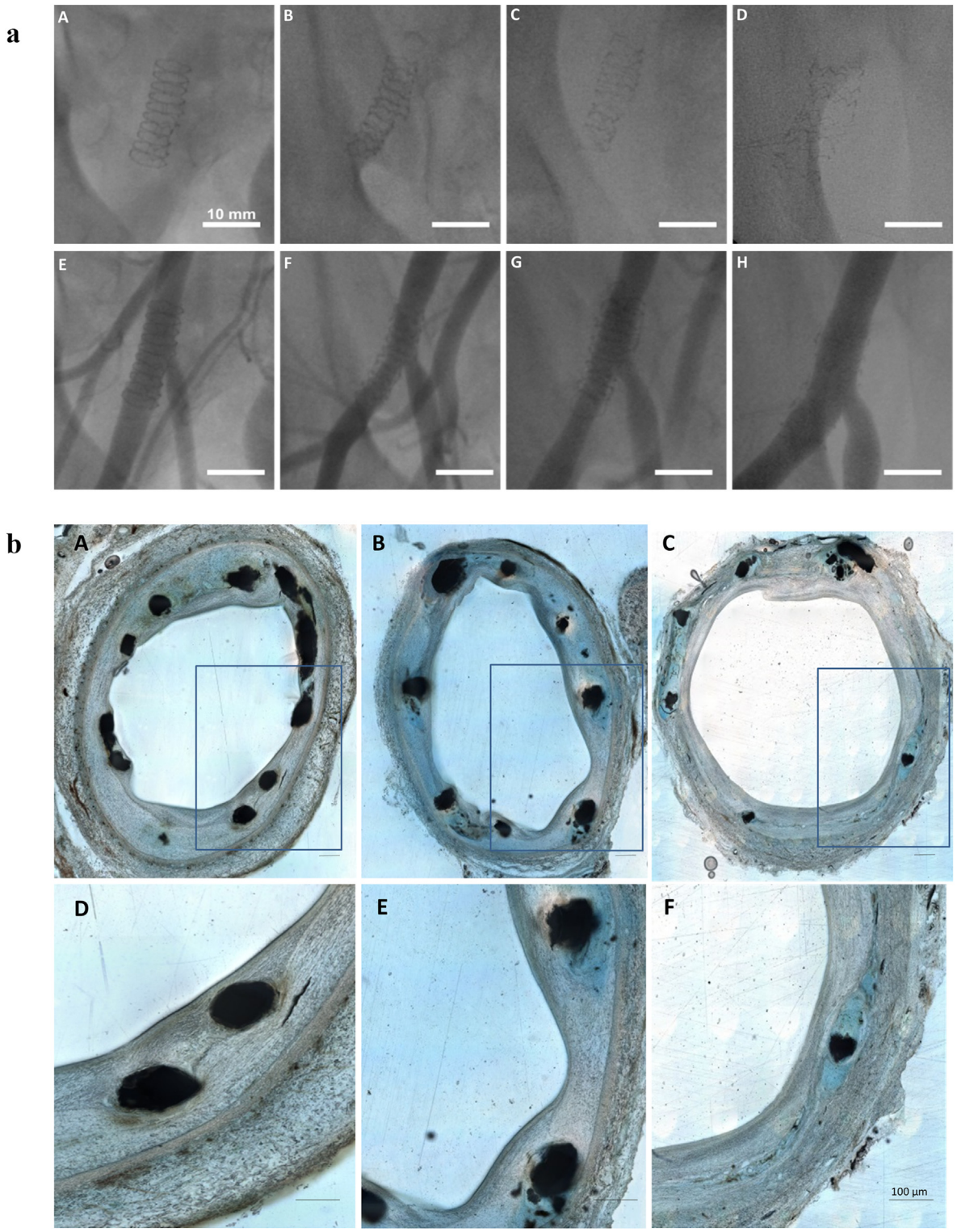

Fig. 6. Fluoroscopic X-ray and histologic images of Zn–3Ag BRS in porcine iliofemoral arteries. a) Fluoroscopic X-ray images of Zn–3Ag BRS in porcine iliofemoral arteries. A–D) Images taken immediately after implantation (A), after 1 month (B), 3 months (C), and 6 months (D) showing the loss of radiopacity of the stents over time. E–H) The next row of angiograms taken immediately after implantation (E), after 1 month (F), 3 months (G), and 6 months (H) revealing vessel patency without significant lumen narrowing or stent thrombosis. b) Histologic images of porcine iliofemoral arteries implanted with Zn–3Ag BRS. A–F) Images taken after 1 month (A and D), 3 months (B and E), and 6 months (C and F). Images D–F showed stent struts within the corresponding arterial cross-sections A–C, respectively. Arteries with Zn–3Ag BRS were completely endothelialized at 1-, 3-, and 6-months follow-up. Reproduced under terms of the CC-BY license [190]. Copyright 2019, Hehrlein et al., published by [Public Library Science].

[135]. Mn possesses a suitable degradation rate and low magnetic susceptibility [153]. The potential dynamic tests showed that Mn has a lower electrochemical potential than Fe, and thus shifts Fe corrosion potential to a less noble state, resulting in a higher degradation rate of Fe–Mn alloys [154]. Besides, Fe–Mn alloys possess superior mechanical properties [153]. Studies suggested that Fe will become anti-ferromagnetic when occurring in the austenitic structure, which can be stabilized by alloying Mn at 25 °C [155]. Biocompatibility assays indicated that Fe–Mn alloys reduced the viability of murine fibroblast cells (L929) and ECV304 cell lines [141]. Therefore, the cytocompatibility of Fe–Mn alloys may be a problem for their clinical use. In addition, the excessive surface roughness of Fe–Mn alloys is unsuitable for stent implantation [154]. Adding a third element to produce a Fe–Mn-X alloy may improve Fe–Mn alloys properties, such as palladium (Pd), copper (Cu), and Ca [155]. However, the addition of these components may also lead to the reduced biocompatibility of Fe–Mn-X alloys [155]. Therefore, further studies are required to focus on measures to improve the surface roughness without sacrificing the biocompatibility of Fe–Mn alloys. Pd and platinum (Pt) have a higher nobility and are soluble in Fe [152]. Studies suggested that the addition of Pd or Pt can improve the mechanical properties, increase the corrosion rate of Fe, and stabilize Fe in austenite form [156]. Gold (Au) is one of the noblest metals with negligible cytotoxicity but is partially soluble in Fe [141]. Silver (Ag) is a promising candidate alloying element due to its anti-bacterial properties and good biocompatibility [157]. Ag has higher electrochemical potential but is not soluble in Fe. It has been shown that Fe–Au and Fe–Ag alloys have faster degradation rates without increasing cytotoxicity, platelet adhesion, or thrombosis effect [157]. Nitrogen (N) is also a promising component added to Fe-based stents. Iron nitride possesses a faster degradation rate and better mechanical properties [158]. It has been suggested that iron nitride stents are fully biocompatible without eliciting systemic toxicity [143]. Moreover, the re-endothelialization was completed within 1 month.

Coating Fe-based stents is another potential approach to optimize their properties. Evidence from recent studies has demonstrated the higher corrosion rate of the iron stents with the bioresorbable polymer coatings [14,16,32]. As polymers such as PLA degrade, alterations occur in the local micro-environment around the implantation sites [159]. Studies have shown promising results in Fe-based stents with PLA coating, also known as metal-polymer composite stent (MPS) [32]. PLA has controllable degradation profiles while the mechanical strength is weak [160]. Thus, MPS combine the superior mechanical properties of Fe and the appropriate degradation behavior of PLA [145]. *In vivo* experiments have shown that the complete degradation of Fe-based MPS with a PLA coating has been achieved in 3–6 months [32]. The MPS was designed on the premise that Fe degrades faster in an acidic environment [32]. Thus, the accelerated degradation rate of MPS might be attributed to the generation of H^+ [14]. In addition, PLA can be hydrolyzed to terminal carboxyl groups, lactate, and H^+, reducing local pH and acidifying the local environment of the stent surface [161]. Apart from the acidification of the surrounding environment, PLA coatings do not prevent sufficient penetration of water, dissolved oxygen, and Cl^- onto the stent surface [162]. Furthermore, a passivation layer mainly composed of Ca and phosphorus (P) is formed after Fe-based stent implantation, hindering the permeation of oxygen onto the stent surface, and slowing down the oxygen reduction [145]. *In vivo* studies have shown that PLA coatings can alleviate the formation of the passivation layer [145]. Moreover, the corrosion rate can be regulated by increasing the amount of PLA or using PLA with lower molecular weight [163]. However, the deposition of the degradation products may result in inflammatory responses and neo-intimal proliferation [164]. Moreover, the alteration of local pH also results in a higher risk of IRS [164]. A recent study introduced a novel stent with great properties. Shen et al. presented a novel poly-DL-lactic acid (PDLLA)-Zn-FeN bioresorbable scaffold with a nanoscale Zn layer between the sirolimus coating and the nitride Fe platform [165]. The *in vivo* degradation behavior of this novel stent occurred in multiple stages. At the early stage after implantation, the PDLLA-Zn-FeN BRS could maintain their mechanical integrity. In human coronary arteries and rabbit abdominal aortas, PDLLA-Zn-FeN BRS showed an increased degradation rate at the subsequent stage. Total degradation (100%) of PDLLA-Zn-FeN BRS occurred in ~2 years. The thickness of the sacrificial Zn layer is adjustable, contributing to the controllable degradation behavior of PDLLA-Zn-FeN BRS and the strong radial strength similar to current permanent stents [165].

Improving the manufacturing process could also optimize the properties of Fe-based stents. The equal-channel angular pressure (ECAP) can produce nanocrystalline Fe with better inhibition of VSCM proliferation but promotes the growth of ECs [166]. The electroforming process was applied to improve the degradation rate of Fe-based stents due to the fine grains and microstructural defects, leading to the increased release of Fe^{2+} [167]. Meanwhile, Fe-based stents produced by powder metallurgy (PM) possess a faster corrosion rate because of the production of more porosity processed by PM [168]. Some novel manufacturing approaches, including inkjet 3D printing and cold gas-dynamic spraying [169], have also shown potential to improve the degradation rate of Fe-based stents. Surface modification is another promising process to optimize stents. Through plasma immersion ion implantation and deposition (PIIID), thin Fe–O films can be constructed to cover the Fe-based stents, which improves the biocompatibility and the mechanical activation of platelets properties [170]. The Fe–O films can reduce the adhesion of activated platelets and promote the proliferation and migration of human umbilical vein endothelial cells (HUVECs), contributing to inhibition of thrombosis and acceleration of re-endothelialization [171]. Apart from PIIID, other surface modifications may also play a role to improve the corrosion rate of Fe-based stents, such as photolithography and electron beam evaporation of platinum discs, sandblasting, phosphating, alkaline heat, MAO and electrodeposition [172]. However, these techniques still require further exploration in the future.

In conclusion, Fe is one of the best potential materials to create biodegradable metallic stents due to its excellent mechanical properties and biocompatibility. Future challenges mainly focus on the improvement of its degradation rate without simultaneously sacrificing its mechanical properties.

3.3. Zn-based stents

3.3.1. Properties of zn-based stents

Zn is an essential trace element in the human body and plays an important role in cell proliferation [173]. Its applications in BRS have shown promising results in a recent study with healthy artery remodeling occurring during stent degradation, and no obvious thrombosis, intimal hyperplasia, and inflammation evident [174]. Zn-based stents have good elongation, appropriate flexural strength, anti-proliferative properties, and most importantly, an ideal degradation rate [173]. From *in vivo* corrosion tests, Zn-based stents could maintain mechanical integrity for ~6 months because of a corrosion-resistant oxide film covering the stent surface [175]. Subsequently, the corrosion process was accelerated and ~50% of stents degraded after 12 months [175]. During corrosion, solid $Zn(OH)_2$ and ZnO are produced with negligible H^+ release [176]. In some preclinical trials assessing the local tissue response to the Zn-based stents, no local or systematic toxicity was observed. In addition, thrombosis, neo-intimal hyperplasia, VSMC proliferation, and inflammation were all in the accepted range, indicating suitable biocompatibility of Zn-based stents [173]. Moreover, Zn also showed a potential anti-bacterial effect [177].

However, the tensile strength of Zn-based stents is too low to provide sufficient mechanical support for blood vessels [178]. Furthermore, some scientists also found that zinc ions (Zn^{2+}) may exert a two-phase effect on vascular cells [179]. At low concentration, Zn^{2+} promoted VSMC proliferation and migration, while yielding the opposite effects at high concentration [179]. Thus, further studies are required to assess the safety and biological effects of Zn-based stents [180].

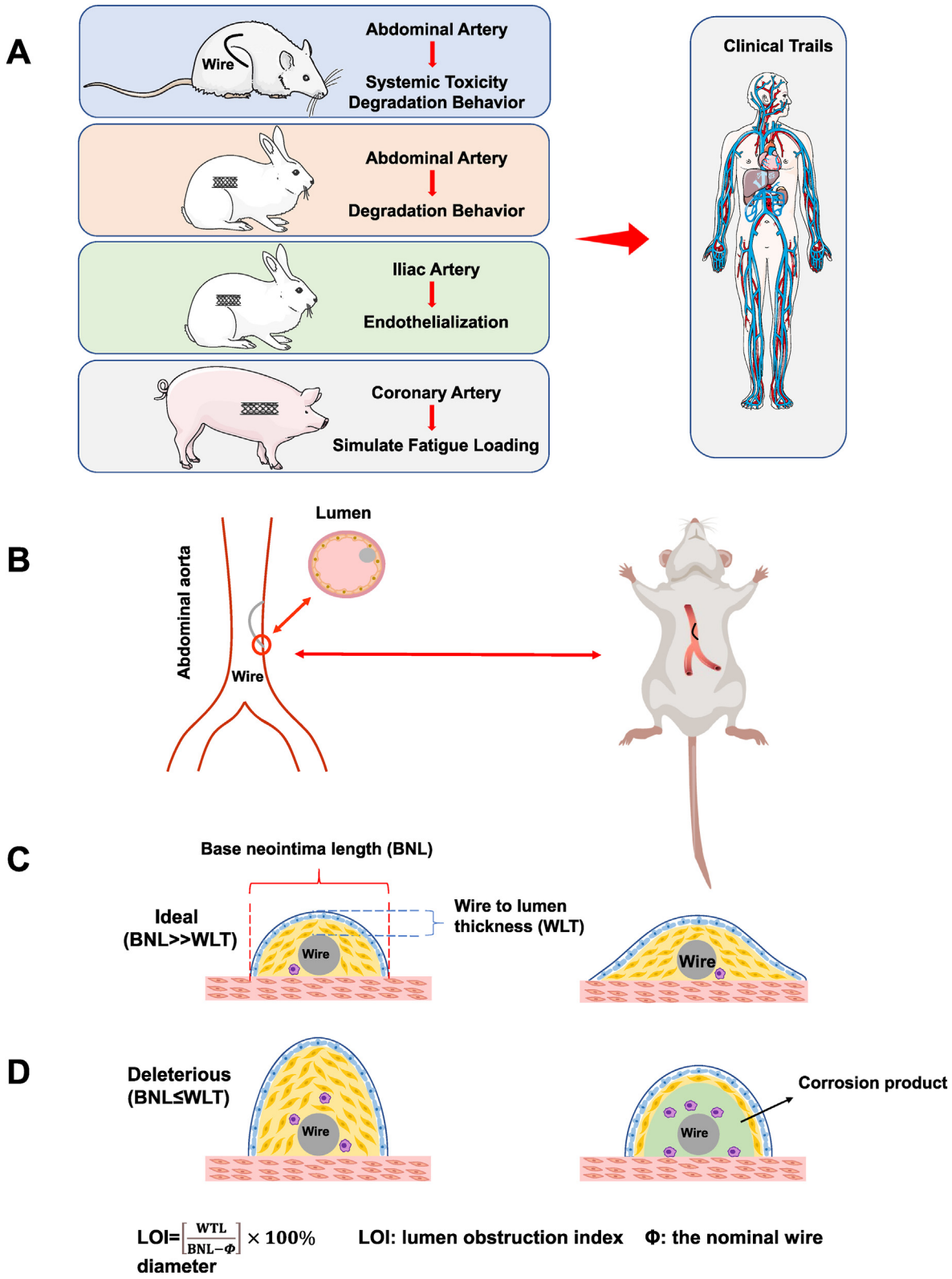

Fig. 7. In vivo animal studies. A) Different animal models which most resemble the performance of humans: 1) Abdominal arteries of rodent animals to evaluate systemic toxicity and degradation behavior; 2) New Zealand rabbit abdominal aorta to evaluate *in vivo* degradation; 3) New Zealand rabbit iliac artery to evaluate the extent of re-endothelialization and EC function restoration; 4) porcine coronary to simulate the release of degradation products and the fatigue loading of the human coronary artery. B) A murine-based wire implant model: different materials are drawn into metal wires and inserted into the abdominal aortic wall or lumen of adult rats to mimic stent implantation. C–D) Two neo-intima types and the morphometric measurement locations concerning the neo-intimal formation. For BNL, the first elastic fiber is traced until negligible neo-intimal activation is observed. WLT is measured near the apex of the neo-intima, at the point where the tissue protrudes furthest into the lumen. A lumen obstruction index (LOI) was developed to quantify the direct success or failure of candidate materials and describe negative histomorphometric appearances. Reproduced with permission [191]. Copyright 2021, Elsevier.

Table 4
Summary of common animal models for BRS investigation.

Species	Common animal models	Advantages	Limitations	Application
Pig	Pig coronary artery model; Minipig coronary artery model	Allowing implantation of human coronary stent; Allowing quantitative angiography and intra-coronary imaging (e.g., IVUS and OCT); Metabolism, cardiovascular and inflammatory system similar to human; Better simulating the release of degradation products and the fatigue loading of the human coronary artery; Pathologic preconditions available (e.g., myocardial infarction model); Knockout/-in available in minipigs	Difficult to care and high expense of feeding	Evaluate ISR and stent safety; Study pharmacokinetics
Rabbit	Rabbit iliac artery model; Rabbit abdominal aorta model;	Iliac arteries similar in size to human coronary arteries, allowing the implantation of human stents; Implanting stents in both iliac arteries, generating contralateral control arteries; Pathologic preconditions available (e.g., atherosclerosis in hypercholesterolemic rabbits); Lipid metabolism and plaque formation similar to human	Lesions consist mainly of lipid-laden macrophages; High requirements for space and care	Evaluate ISR, *in vivo* degradation behavior (abdominal aorta) and the extent of re-endothelialization and EC function restoration (iliac artery)
Mouse	Murine aorta model	High genetic manipulability (e.g., ApoE$^{-/-}$ and LDL$^{-/-}$); Low requirements for space and care; Plenty of different strains available; Pathologic preconditions available; Similar immune system to humans	Too small for stent implantation; Difficult to develop high-risk plaques	Evaluate ISR; *in vivo* degradation behavior and systemic toxicity
Rat	Rat carotid artery model; Rat abdominal aorta model; Rat common iliac artery model	Large enough for stent implantation; Low requirements for space and care; Pathologic preconditions available;	Different lipid metabolism compared to human; Plaque formation is different from humans; Fewer transgenic models compared to mice	Pharmacological tests and metabolic manipulation; Evaluate *in vivo* degradation behavior and systemic toxicity
Dog	Canine coronary artery model; Canine carotid artery model	Large enough for stent implantation; Easy handling	Not allow for genetic manipulation; High requirements for space and care; Different immune system and lipid metabolism compared to human;	Evaluate stent safety and efficacy
Primates	Primate carotid artery model; Primate aorta model	Most closely evolutionarily related to humans (e.g., similar metabolism, immune system, and cardiovascular system); Large enough for stent implantation; Knockout/-in available in some primates (e.g., Cynomolgus and Rhesus);	High ethical hurdles; Very high costs on husbandry;	Very limited use

3.3.2. *Optimization and future challenges of Zn-based stents*

Although Zn has insufficient mechanical strength for stent implantation, its ideal degradation rate and suitable biocompatibility have motivated scientists to optimize Zn-based stents with improved tensile strength primarily through alloying [181]. It has been proven that Zn alloys can maintain their mechanical strength during the early implantation time [173]. Researchers found that the tensile strength of Zn–Mg alloys is markedly improved. However, the addition of Mg also led to the reduced biocompatibility of Zn–Mg alloys, e.g., slightly elevated inflammatory responses and neo-intimal hyperplasia [182]. Adding another element into the Zn–Mg system results in further improvement of the properties of the alloy. Lin et al. inserted a Zn–Mg–Cu scaffold into a rabbit carotid artery to evaluate the properties of this stent [183]. They found that the Zn–Mg–Cu alloy had stronger mechanical strength, compatible degradation rate, and rapid re-endothelialization rate [183]. Similar to the Zn–Mg alloys, Zn–Al alloys also possess stronger mechanical strength. However, studies have shown that after the implantation of Zn–Al alloys, acute and chronic inflammatory responses could be identified, indicating Al may provoke toxicity to adjacent cells and tissues [184]. In addition, the mechanical and degradation properties of Zn–Al alloys can be further improved by adding other elements like Cu, Mg, Ca, and Sr [185]. In contrast to other Zn alloys, Zn–Al alloys exhibited intergranular corrosion, which may embrittle the alloy in the vascular micro-environment, promoting fragmentation of the Zn–Al alloy stents [186]. It is well acknowledged that silver ions (Ag^{+}) can kill bacteria that adhere to the stent surface or inhibit bacterial adhesion, decreasing the incidence of stent-related infections [187]. Accordingly, Zn–Ag alloys are of great interest for anti-bacterial stents to reduce mortality caused by stent-related infections [188]. Zn–Ag alloys have good mechanical strength that can be variably tailored by adjusting the Ag content [189]. Furthermore, Zn–Ag alloys were successfully fabricated into an ultrathin structure with a sirolimus coating to reduce the neo-intimal formation [120]. However, excessive enrichment of Ag and corrosion products like $AgZn_3$ at the interface may induce problematic cytotoxicity, affecting the vascular remodeling process [176]. In 2018, Hehrlein et al. implanted a novel Zn–3Ag BRS into porcine iliofemoral arteries with enhanced ductility and higher tensile strength compared to PLLA and Mg [190]. After implantation, the Zn–3Ag BRS was easily visible fluoroscopically and their biodegradation process was detectable via X-ray over time (Fig. 6A). The results showed that there were no signs of early thrombosis and only minor lumen stenosis occurred at 1-, 3-, and 6-months follow-up. In addition, histologic data revealed that arteries with a Zn–3Ag BRS were completely covered with neo-intima without ST or vascular occlusion, thus maintaining vascular scaffolding for a minimum period of 6 months (Fig. 6B). Furthermore, Zn–3Ag BRS also had moderate degradation rates [190]. Thus, the Zn–3Ag BRS is a promising material platform as a new generation of vascular stents, which requires further investigation. Similar to Zn–Ag alloys, Zn–Cu stents implanted into the pig coronary arteries exhibited a suitable re-endothelialization rate and positive vascular remodeling as the stent degraded [182].

However, alloying can also lead to poor ductility and low strength of Zn-based alloys [181]. Apart from alloying, material modifications affect the properties of Zn stents [191]. For instance, grain refinement induced by thermomechanical treatments can further improve the mechanical characteristics of cast Zn alloys [176]. In addition, severe plastic deformation techniques may tailor the mechanical properties of Zn alloys [27].

The main challenge with Zn-based stents lies in the optimization of the elemental composition and processing route to achieve better microstructural characteristics and mechanical strength needed for cardiovascular stents without sacrificing its perfect *in vivo* degradation properties and suitable biocompatibility.

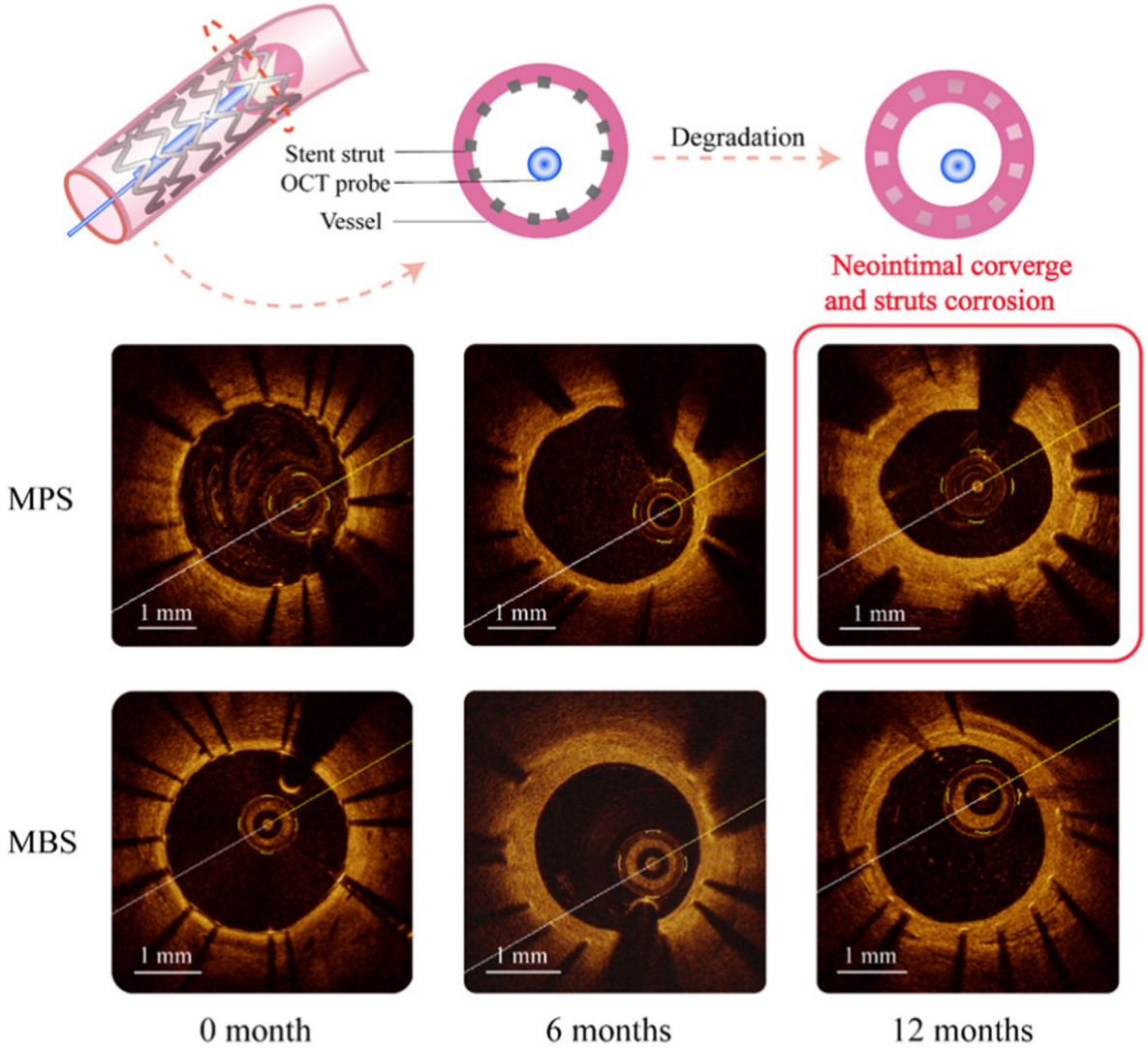

Fig. 8. Schema of OCT imaging and OCT images of MPS and MBS implanted into porcine coronary arteries. Compared to MBS, MPS exhibited obviously wider struts after 12 months of implantation. OCT results showed that MPS degraded faster than MBS. Reproduced with permission [14]. Copyright 2020, American Chemical Society.

4. Bioresorbable electronic stents

After BRS implantation, it is hard to evaluate the internal status and the potential risks. However, bioresorbable electronic stents, comprising scaffolds with biodegradable and flexible electronics, can convey information about their status [18]. Therefore, the status of the stent can be readily assessed for timely treatment to reduce adverse events [18].

Takahata et al. developed an antenna stent (stentenna) that can monitor flow and pressure in the lumen through a wireless connection to an *in vitro* micromechanical stent-like structure [192]. Subsequently, Chow et al. proposed a revolutionary concept of a medical stent combined with a completely wireless implantable cardiac monitor [193]. The stent can provide structural support for blood vessels while serving as a wireless telemetry and power antenna. It can also detect and communicate cardiovascular status. Specifically, it can detect restenosis or re-occlusion in advance [193].

In BDMS (e.g., Mg), ions can act as antenna backbones due to their appropriate conductivity. Son et al. fabricated an Mg-based bioresorbable electronic stent, which can function as a data wireless interlocutor [194]. This is because the Mg alloy is conductive as an antenna unit. The scaffold also shows excellent functions; e.g., a memory module and a blood-flow/temperature sensor. Despite these advantages, active electronic components have a high degradation rate. Son et al. used an encapsulation layer of PLA and MgO to retard the degradation process but the results remain unsatisfactory [194]. Therefore, it is critical to slow down the degradation of BDMS to maintain their conductivity.

Conductive polymers possess high electrical conductivity and fascinating properties; e.g., processability and easy synthesis [195]. Common conductive polymers include polythiophene (PT), polyaniline (PANi), polypyrrole (PPy), and polyacetylene (PAC). However, these conductive polymers are not biodegradable or biocompatible and show poor mechanical properties. Polymer blends composed of biodegradable polymers (e.g., PLA) and conducting polymers can potentially overcome these drawbacks, and their combination warrants further investigation.

Ding et al. have developed a bioresorbable, flexible, and conductive metal-polymer conductor (MPC) [196]. The external MPC stent (MPCS) can electroporate the vessel wall and produce a protein to inhibit intimal hyperplasia (IH) [196]. Electroporation provides a safer and more effective path for functional gene delivery as compared to viral vectors. MPCS can also provide mechanical support for vein grafts (VGs). This device provides novel insights into the development of bioelectronics for electroporation gene therapy.

5. *In vivo* models and experiments to analyze BRS properties

Scientists have made great efforts to simulate *in vivo* environments for evaluation of the properties of BRS as *in vitro* models are oversimplified [197]. The complex interactions between blood, proteins, cells, and stents, shear stress of blood flow as well as vasomotion all play roles in the degradation behavior [178]. In addition, some conditions cannot be replicated *in vitro*, such as the complicated signaling between the initial coagulation cascade and subsequent cell responses [198]. Studies have shown that the degradation rate and the degradation products are different between *in vitro* and *in vivo* conditions [199]. Therefore, it is necessary to improve *in vivo* models similar to human vessels for evaluation of stent performance especially degradation behavior and endothelial function, to translate preclinical results into clinical practice. Normally, one animal model is hard to accurately predict all the conditions after implantation in humans; therefore, it is suggested that different animal models should be used to guide stent design iteration before clinical use (Fig. 7A) [200]. The advantages and limitations of common animal models are summarized in Table 4.

5.1. *In vivo evaluation of BRS degradation behavior*

5.1.1. *Possible factors influencing degradation behavior of BRS in vivo*

The stent has complex interactions with the blood vessel cells, thereby influencing hemodynamics in the lumen and altering the mechanical micro-environment within the host vessels after its implantation [201]. Replicating realistic physiological conditions is significant to evaluate the clinical transformation of BRS. *In vivo* studies have proven that the degradation rate is lower for the stents inserted in the arterial lumen as compared to those on the arterial wall [202]. The result may shed light on the importance of dynamic blood flow on the degradation behavior of BRS and promote the development of *in vivo* blood-contacting models for assessing degradation rate. Apart from the blood flow, cells and proteins also affect the degradation behavior of implanted stents *in vivo* [201]. These results implicate the significance of evaluating the degradation rates of stents in different *in vivo* models before clinical trials.

5.1.2. *Approaches for evaluating the degradation behavior of BRS in vivo*

Several methods have been applied to evaluate the degradation behavior of BRS *in vivo*. Weight-loss measurement is a quantitative, reliable approach, whereby residual mass and radial strength of the stents after implantation are measured [203]. Additionally, analyzing degradation product and surface topography can facilitate the evaluation of degradation behavior *in vivo*. Pierson et al. have developed a novel *in vivo* model by implanting a biomaterial wire into the artery lumen/wall of rats (Fig. 7B) [202]. Using scanning electron microscopy (SEM), energy dispersive spectroscopy (EDM), and Raman spectroscopy, they have evaluated the degradation behavior of Fe and Mg wires. Notably, this wire implantation model allows *in vivo* evaluation of candidate BRS materials without the need for implantation of costly and specialized fabricating stents into animals. Bowen et al. have implanted Zn wires into the abdominal aorta of rats to assess *in vivo* degradation behavior [204]. Back-scattered-electron section imaging was performed to scan several cross sections from explanted samples. By measuring the average penetration rates and cross-sectional area reduction, *in vivo* degradation behavior of Zn wires was quantified.

However, the above methods are destructive, and the removal of wires or stents is inevitable. Thus, these have not been evaluated in any clinical trial. Non-destructive methods like OCT, IVUS, and micro-CT are not quantitative and provide only a rough estimate of *in vivo* biodegradation. In 2020, Li et al. used OCT to evaluate *in vivo* degradation behavior of a Fe-based MPS with a PLA coating relative to the corresponding metal-based stent (MBS) [14]. The results showed that MPS degraded faster than MBS [14]. OCT images of MPS and MBS are presented in Fig. 8. However, non-quantitative methods remain limited to the clinical trial phase. To establish a non-destructive but semi-quantitative method to evaluate *in vivo* degradation behavior of BRS, Lin et al. developed a semi-quantitative modality based on OCT [16]. They implanted a Fe-based stent with an asymmetric sirolimus-loaded PDLLA coating into Bama minipig coronary arteries and New Zealand rabbit abdominal aortas to evaluate the *in vivo* degradation behavior. During degradation, Fe corrosion products diffused to the surrounding, thus changing the contour of the luminal surface of the Fe strut into an arched highlight region with the rear shadow in OCT. Thus, the degradation degree (d) of Fe struts can be expressed by the radial height (T) of the bow area in OCT. For semi-quantitative modality, the radial height of $2T_0$ (the initial T) implies 20% Fe degradation (d2); $3T_0$ represents 50% Fe degradation (d3), and $4T_0$ means nearly full degradation (dj) [16]. Compared to the weighing method, the calculated degradation rate by OCT is similar to that of the weight-loss method, indicating the high accuracy of this semi-quantitative method. Moreover, repeatability and reproducibility were acceptable for OCT with a maximum standard deviation less than 3.1 wt % and maximum relative standard deviation less than 8.4% [16]. Taken together, this novel non-destructive method to evaluate *in vivo* degradation performance of BRS has significant implications for late-stage clinical trials and follow-up.

5.2. *In vivo endothelial coverage, endothelial function restoration, and neo-intimal response evaluation*

The New Zealand rabbit iliac artery model was applied to evaluate the extent of re-endothelialization and EC function restoration [16]. Several antibodies are required to stain stents: VE-Cadherin for endothelium with mature junctional complexes [205], P120 for endothelium without mature junctional complexes [206], and DAPI for nuclear counterstain [207]. Three possible areas can be observed in this analysis: (1) Competent barrier-forming ECs: VE-Cadherin co-localized with P120 at cell borders; (2) Non-functional endothelium: only P120 localized to cell borders; (3) Uncovered: no VE-Cadherin or P120 [16]. Based on the functional endothelial coverage test, re-endothelialization is defined as the percentage of area with competent barrier-forming ECs, providing novel insights for *in vivo* evaluation of the extent of re-endothelialization and EC function restoration.

In 2019, Guillory et al. used the wire implantation model as a quantitative neo-intimal morphometric method to evaluate the biocompatibility of BRS by measuring thickness, area, and protrusion into the arterial lumen of neo-intima tissue surrounding the wire implant [208]. To evaluate the biocompatibility of degradable materials, several neo-intimal morphometric metrics were introduced, such as NA, base neo-intimal length (BNL) and wire lumen thickness (WLT) [208]. According to these indicators, the lumen occlusion index (LOI) was calculated to clinically evaluate stents as an indicator of diameter stenosis (Fig. 7C and D). Guillory et al. suggested that implant failure should be defined as WLT >70 μm or LOI $>30\%$ [208]. Many preclinical experiments utilize this murine-based wire implantation model to evaluate the effects of the BRS material class, surface treatment, degradation byproducts, alloying, manufacturing processes and microstructure on the neo-intimal response [84,175,178].

6. Conclusions and future perspectives

The introduction of the concept of BRS brings both opportunities and challenges to the field of coronary interventions. DES dominates the coronary stent market; however, it has several deficiencies, including inhibition of normal coronary vasomotion at a late stage and provoking long-term inflammatory responses [197]. The transient BRS is expected to overcome the limitations of DES. During degradation, the absorption of BRS potentially helps improve the positive remodeling of coronary arteries, preserve vasoreactivity, reduce the incidence of LST due to the absence of foreign materials, and inhibit edge vascular response (i.e.,

luminal narrowing at stent edges) [209,210]. Based on completed clinical trial results, BRS shows great potential as the next-generation stents; however, there are also some limitations to BRS in clinical applications. Although the mechanical properties of BRS are close to that of BMS/DES *in vitro*, evidence from *in vivo* and human studies demonstrates a decreased focal radial expansion of BRS, especially without routine post-dilatation [210,211]. The radial strength of BRS has been a problem, especially for polymeric ones. Designing BRS with a thicker strut to compensate for the insufficient mechanical strength is not a final solution. High strut thickness may inhibit the healing process and increase the incidence of stent malapposition due to fracture in its integrity during degradation [197]. Therefore, further studies are needed to better balance the strut thickness and radial strength. Based on the clinical trials that have been completed thus far, the incidence of clinical events for patients treated with BRS is similar to those treated with DES, except for a worse LLL in BRS [212]. This suggests that the restoration of vascular physiological function may partially counterbalance some of the drawbacks of BRS.

Although improved implantation protocols for BRS may lead to better clinical outcomes to some extent, failure to obtain FDA approval suggests the significance of developing optimal biodegradable materials and advanced manufacturing techniques. The examination of novel BRS materials should focus on the balance among endothelialization, degradation behavior, mechanical properties, and biocompatibility. Additionally, the development of appropriate *in vivo* models is also important for the evaluation of novel BRS materials before clinical trials. The currently used *in vivo* models have defects due to the physiological differences between animals (e.g., pigs, rabbits, and rats) and humans. Therefore, positive results in animal experiments cannot be directly translated to human findings [213]. These differences include faster regeneration in animals, differences in the blood chemistry, re-endothelialization rates, and total cellular profiles, along with a lack of phenotypic heterogeneity in laboratory strains among pigs, rabbits, and rodents [213]. In addition, most animal experiments are performed in healthy animals, while a stent is commonly susceptible to different vessel conditions with varying lesions in the progressive CADs [213]. Moreover, the latest assessment methods available to patients in the clinic, such as OCT, must be evaluated in animal experiments [15]. Recent studies have supported the accuracy of OCT for the evaluation of the degradation rate of BRS [16]. In the future, further studies are required to develop appropriate *in vivo* models and apply novel clinical technologies to evaluate BRS properties in animals. Through advanced manufacturing techniques, especially the development of SMPs, 3D printing, and biosensors, BRS is expected to possess unprecedented features, including remote self-monitoring, precise adaptation to blood vessels, and shape change [21]. Applying 3D printing into shape-memory materials implements adaptive functionality, thus allowing for the physical transformation of 3D-printed stents over time to perform programmed tasks. Additionally, advancements in intracoronary imaging guidance are also needed to improve clinical outcomes [213].

Finally, to maximize the advantages and potentials of BRS, multidisciplinary studies are needed in the future. Based on current evidence from *in vivo* assays and clinical trials, the design of next-generation BRS should focus on the following aspects: greater mechanical strength to avoid recoil, decreased strut thickness, and developing novel technologies (e.g., 3D printing and biosensor) to allow real-time detection, responses, and adaption to environmental changes [21,197]. With the exciting and continual advancements in technologies, developing a next-generation BRS may improve the efficacy of treatments for CADs in the future.

Author statement

Jiabin Zong, Quanwei He and Jiehong Wu contributed equally to this work.

Jiabin Zong: Conceptualization, Writing – original draft, Writing – review & editing. **Quanwei He**: Conceptualization, Funding acquisition, Writing – review & editing. **Yuxiao Liu**: Writing – original draft. **Min Qiu**: Writing – original draft. **Jiehong Wu**: Conceptualization, Funding acquisition, Supervision, Writing – original draft, Writing – review & editing. **Bo Hu**: Conceptualization, Funding acquisition, Supervision, Writing – review & editing.

Declaration of competing interest

The authors declare that they have no known competing financial interests or personal relationships that could have appeared to influence the work reported in this paper.

Acknowledgements

All authors have read the journal's authorship statement. The manuscript was reviewed and approved by all named authors. This work was supported by National Natural Science Foundation of China (No. 82090044 to B.H, No. 82001271 to J.H.W, No. 81820108010 to B.H, No. 82071335 to Q.W.H). We thank Bullet Edits Limited for the linguistic editing and proofreading of the manuscript.

References

[1] S.S. Virani, A. Alonso, E.J. Benjamin, M.S. Bittencourt, C.W. Callaway, A.P. Carson, A.M. Chamberlain, A.R. Chang, S. Cheng, F.N. Delling, L. Djousse, M.S.V. Elkind, J.F. Ferguson, M. Fornage, S.S. Khan, B.M. Kissela, K.L. Knutson, T.W. Kwan, D.T. Lackland, T.T. Lewis, J.H. Lichtman, C.T. Longenecker, M.S. Loop, P.L. Lutsey, S.S. Martin, K. Matsushita, A.E. Moran, M.E. Mussolino, A.M. Perak, W.D. Rosamond, G.A. Roth, U.K.A. Sampson, G.M. Satou, E.B. Schroeder, S.H. Shah, C.M. Shay, N.L. Spartano, A. Stokes, D.L. Tirschwell, L.B. VanWagner, C.W. Tsao, E. American Heart Association Council on, C. Prevention Statistics, S. Stroke Statistics, Heart disease and stroke statistics-2020 update: a report from the American heart association, Circulation 141 (9) (2020) e139–e596, https://doi.org/10.1161/CIR.0000000000000757.

[2] N. Beshchasna, A.Y.K. Ho, M. Saqib, H. Kraskiewicz, L. Wasyluk, O. Kuzmin, O.C. Duta, D. Ficai, R.D. Trusca, A. Ficai, V.F. Pichugin, J. Opitz, E. Andronescu, Surface evaluation of titanium oxynitride coatings used for developing layered cardiovascular stents, Mater Sci Eng C Mater Biol Appl 99 (2019) 405–416, https://doi.org/10.1016/j.msec.2019.01.131.

[3] C. Haben, W.M. Park, J.F. Bena, F.E. Parodi, S.P. Lyden, Improving midterm results justify the continued use of bare-metal stents for endovascular therapy for chronic mesenteric ischemia, J. Vasc. Surg. 71 (1) (2020) 111–120, https://doi.org/10.1016/j.jvs.2019.01.094.

[4] Y. Chen, P. Gao, L. Huang, X. Tan, N. Zhou, T. Yang, H. Qiu, X. Dai, S. Michael, Q. Tu, N. Huang, Z. Guo, J. Zhou, Z. Yang, H. Wu, A tough nitric oxide-eluting hydrogel coating suppresses neointimal hyperplasia on vascular stent, Nat. Commun. 12 (1) (2021) 7079, https://doi.org/10.1038/s41467-021-27368-4.

[5] B.E. Claessen, J.P. Henriques, F.A. Jaffer, R. Mehran, J.J. Piek, G.D. Dangas, Stent thrombosis: a clinical perspective, JACC Cardiovasc. Interv. 7 (10) (2014) 1081–1092, https://doi.org/10.1016/j.jcin.2014.05.016.

[6] A. Sambola, P. Rello, T. Soriano, D.L. Bhatt, V. Pasupuleti, C.P. Cannon, C.M. Gibson, W.J.M. Dewilde, G.Y.H. Lip, E.D. Peterson, K.E.J. Airaksinen, T. Kiviniemi, L. Fauchier, L. Raber, J.M. Ruiz-Nodar, M. Banach, H. Bueno, A.V. Hernandez, Safety and efficacy of drug eluting stents vs bare metal stents in patients with atrial fibrillation: a systematic review and meta-analysis, Thromb. Res. 195 (2020) 128–135, https://doi.org/10.1016/j.thromres.2020.07.010.

[7] M.L. Tsai, M.J. Hsieh, C.C. Chen, S.H. Chang, C.Y. Wang, D.Y. Chen, C.H. Yang, J.K. Yeh, M.Y. Ho, I.C. Hsieh, Comparison of 9-month angiographic follow-up and long-term clinical outcomes of biodegradable polymer drug-eluting stents and second-generation durable polymer drug-eluting stents in patients undergoing single coronary artery stenting, Acta Cardiol. Sin. 36 (2) (2020) 97–104, https://doi.org/10.6515/ACS.202003_36(2).20190729A.

[8] G. De Luca, P. Smits, S.H. Hofma, E. Di Lorenzo, G.J. Vlachojannis, A.W.J. Van't Hof, A.J. van Boven, E. Kedhi, G.W. Stone, H. Suryapranata, c. Drug-Eluting Stent in Primary Angioplasty, Everolimus eluting stent vs first generation drug-eluting stent in primary angioplasty: a pooled patient-level meta-analysis of randomized trials, Int. J. Cardiol. 244 (2017) 121–127, https://doi.org/10.1016/j.ijcard.2017.06.022.

[9] S. Torii, H. Jinnouchi, A. Sakamoto, M. Kutyna, A. Cornelissen, S. Kuntz, L. Guo, H. Mori, E. Harari, K.H. Paek, R. Fernandez, D. Chahal, M.E. Romero, F.D. Kolodgie, A. Gupta, R. Virmani, A.V. Finn, Drug-eluting coronary stents: insights from preclinical and pathology studies, Nat. Rev. Cardiol. 17 (1) (2020) 37–51, https://doi.org/10.1038/s41569-019-0234-x.

[10] R. Yue, J. Niu, Y. Li, G. Ke, H. Huang, J. Pei, W. Ding, G. Yuan, In vitro cytocompatibility, hemocompatibility and antibacterial properties of biodegradable Zn-Cu-Fe alloys for cardiovascular stents applications, Mater Sci Eng C Mater Biol Appl 113 (2020), 111007, https://doi.org/10.1016/j.msec.2020.111007.

[11] N. Beshchasna, M. Saqib, H. Kraskiewicz, L. Wasyluk, O. Kuzmin, O.C. Duta, D. Ficai, Z. Ghizdavet, A. Marin, A. Ficai, Z. Sun, V.F. Pichugin, J. Opitz, E. Andronescu, Recent advances in manufacturing innovative stents, Pharmaceutics 12 (4) (2020), https://doi.org/10.3390/pharmaceutics12040349.

[12] W.A. Omar, D.J. Kumbhani, The current literature on bioabsorbable stents: a review, Curr. Atherosclerosis Rep. 21 (12) (2019) 54, https://doi.org/10.1007/s11883-019-0816-4.

[13] Y. Sotomi, Y. Onuma, C. Collet, E. Tenekecioglu, R. Virmani, N.S. Kleiman, P.W. Serruys, Bioresorbable scaffold: the emerging reality and future directions, Circ. Res. 120 (8) (2017) 1341–1352, https://doi.org/10.1161/CIRCRESAHA.117.310275.

[14] X. Li, W. Zhang, W. Lin, H. Qiu, Y. Qi, X. Ma, H. Qi, Y. He, H. Zhang, J. Qian, G. Zhang, R. Gao, D. Zhang, J. Ding, Long-term efficacy of biodegradable metal-polymer composite stents after the first and the second implantations into porcine coronary arteries, ACS Appl. Mater. Interfaces 12 (13) (2020) 15703–15715, https://doi.org/10.1021/acsami.0c00971.

[15] J. Li, C. Shang, Y. Rong, J. Sun, Y. Cheng, B. He, Z. Wang, M. Li, J. Ma, B. Fu, X. Ji, Review on laser technology in intravascular imaging and treatment, Aging Dis. 13 (1) (2022) 246–266, https://doi.org/10.14336/AD.2021.0711.

[16] W. Lin, H. Zhang, W. Zhang, H. Qi, G. Zhang, J. Qian, X. Li, L. Qin, H. Li, X. Wang, H. Qiu, X. Shi, W. Zheng, D. Zhang, R. Gao, J. Ding, In vivo degradation and endothelialization of an iron bioresorbable scaffold, Bioact. Mater. 6 (4) (2021) 1028–1039, https://doi.org/10.1016/j.bioactmat.2020.09.020.

[17] N. L'Heureux, N. Dusserre, G. Konig, B. Victor, P. Keire, T.N. Wight, N.A. Chronos, A.E. Kyles, C.R. Gregory, G. Hoyt, R.C. Robbins, T.N. McAllister, Human tissue-engineered blood vessels for adult arterial revascularization, Nat. Med. 12 (3) (2006) 361–365, https://doi.org/10.1038/nm1364.

[18] S.H. Im, Y. Jung, S.H. Kim, Current status and future direction of biodegradable metallic and polymeric vascular scaffolds for next-generation stents, Acta Biomater. 60 (2017) 3–22, https://doi.org/10.1016/j.actbio.2017.07.019.

[19] D. Hoare, A. Bussooa, S. Neale, N. Mirzai, J. Mercer, The future of cardiovascular stents: bioresorbable and integrated biosensor technology, Adv. Sci. 6 (20) (2019), 1900856, https://doi.org/10.1002/advs.201900856.

[20] J. Li, Y. Long, F. Yang, H. Wei, Z. Zhang, Y. Wang, J. Wang, C. Li, C. Carlos, Y. Dong, Y. Wu, W. Cai, X. Wang, Multifunctional artificial artery from direct 3D printing with built-in ferroelectricity and tissue-matching modulus for real-time sensing and occlusion monitoring, Adv. Funct. Mater. 30 (39) (2020), https://doi.org/10.1002/adfm.202002868.

[21] E. Vahabli, J. Mann, B.S. Heidari, M. Lawrence-Brown, P. Norman, S. Jansen, E.J. Pardo, B. Doyle, The technological advancement to engineer next-generation stent-grafts: design, material, and fabrication techniques, Adv. Healthc. Mater. (2022), e2200271, https://doi.org/10.1002/adhm.202200271.

[22] S.A. El-Safty, M.A. Shenashen, Nanoscale dynamic chemical, biological sensor material designs for control monitoring and early detection of advanced diseases, Mater. Today Biol. 5 (2020), 100044, https://doi.org/10.1016/j.mtbio.2020.100044.

[23] R. Khalaj, A.G. Tabriz, M.I. Okereke, D. Douroumis, 3D printing advances in the development of stents, Int. J. Pharm. 609 (2021), 121153, https://doi.org/10.1016/j.ijpharm.2021.121153.

[24] T.R. Yeazel, M.L. Becker, Advancing toward 3D printing of bioresorbable shape memory polymer stents, Biomacromolecules 21 (10) (2020) 3957–3965, https://doi.org/10.1021/acs.biomac.0c01082.

[25] C. Zhang, D. Cai, P. Liao, J.W. Su, H. Deng, B. Vardhanabhuti, B.D. Ulery, S.Y. Chen, J. Lin, 4D Printing of shape-memory polymeric scaffolds for adaptive biomedical implantation, Acta Biomater. 122 (2021) 101–110, https://doi.org/10.1016/j.actbio.2020.12.042.

[26] P.K. Bowen, E.R. Shearier, S. Zhao, R.J. Guillory 2nd, F. Zhao, J. Goldman, J.W. Drelich, Biodegradable metals for cardiovascular stents: from clinical concerns to recent Zn-alloys, Adv. Healthc. Mater. 5 (10) (2016) 1121–1140, https://doi.org/10.1002/adhm.201501019.

[27] E. Mostaed, M. Sikora-Jasinska, J.W. Drelich, M. Vedani, Zinc-based alloys for degradable vascular stent applications, Acta Biomater. 71 (2018) 1–23, https://doi.org/10.1016/j.actbio.2018.03.005.

[28] D.B. Camasao, D. Mantovani, The mechanical characterization of blood vessels and their substitutes in the continuous quest for physiological-relevant performances. A critical review, Mater. Today Biol. 10 (2021), 100106, https://doi.org/10.1016/j.mtbio.2021.100106.

[29] A. Sensini, C. Gualandi, M.L. Focarete, J. Belcari, A. Zucchelli, L. Boyle, G.C. Reilly, A.P. Kao, G. Tozzi, L. Cristofolini, Multiscale hierarchical bioresorbable scaffolds for the regeneration of tendons and ligaments, Biofabrication 11 (3) (2019), 035026, https://doi.org/10.1088/1758-5090/ab20ad.

[30] S. Bangalore, H.G. Bezerra, D.G. Rizik, E.J. Armstrong, B. Samuels, S.S. Naidu, C.L. Grines, M.T. Foster, J.W. Choi, B.D. Bertolet, A.P. Shah, R. Torguson, S.B. Avula, J.C. Wang, J.P. Zidar, A. Maksoud, A. Kalyanasundaram, S.J. Yakubov, B.M. Chehab, A.J. Spaedy, S.P. Potluri, R.P. Caputo, A. Kondur, R.F. Merritt, A. Kaki, R. Quesada, M.A. Parikh, C. Toma, F. Matar, J. DeGregorio, W. Nicholson, W. Batchelor, R. Gollapudi, E. Korngold, R. Sumar, G.S. Chrysant, J. Li, J.B. Gordon, R.M. Dave, G.F. Attizzani, T.P. Stys, O.S. Gigliotti, B.E. Murphy, S.G. Ellis, R. Waksman, The state of the absorb bioresorbable scaffold: consensus from an expert panel, JACC Cardiovasc. Interv. 10 (23) (2017) 2349–2359, https://doi.org/10.1016/j.jcin.2017.09.041.

[31] L.P. Tan, S.S. Venkatraman, J.F. Joso, F.Y. Boey, Collapse pressures of bilayered biodegradable stents, J. Biomed. Mater. Res. B Appl. Biomater. 79 (1) (2006) 102–107, https://doi.org/10.1002/jbm.b.30518.

[32] Y. Qi, H. Qi, Y. He, W. Lin, P. Li, L. Qin, Y. Hu, L. Chen, Q. Liu, H. Sun, Q. Liu, G. Zhang, S. Cui, J. Hu, L. Yu, D. Zhang, J. Ding, Strategy of metal-polymer composite stent to accelerate biodegradation of iron-based biomaterials, ACS Appl. Mater. Interfaces 10 (1) (2018) 182–192, https://doi.org/10.1021/acsami.7b15206.

[33] J.A. Ormiston, P.W. Serruys, E. Regar, D. Dudek, L. Thuesen, M.W. Webster, Y. Onuma, H.M. Garcia-Garcia, R. McGreevy, S. Veldhof, A bioabsorbable everolimus-eluting coronary stent system for patients with single de-novo coronary artery lesions (ABSORB): a prospective open-label trial, Lancet 371 (9616) (2008) 899–907, https://doi.org/10.1016/S0140-6736(08)60415-8.

[34] J. Li, P. Nemes, J. Guo, Mapping intermediate degradation products of poly(lactic-co-glycolic acid) in vitro, J. Biomed. Mater. Res. B Appl. Biomater. 106 (3) (2018) 1129–1137, https://doi.org/10.1002/jbm.b.33920.

[35] S.H. Kang, W.Y. Chung, J.M. Lee, J.J. Park, C.H. Yoon, J.W. Suh, Y.S. Cho, J.H. Doh, J.M. Cho, J.W. Bae, T.J. Youn, I.H. Chae, Angiographic outcomes of Orsiro biodegradable polymer sirolimus-eluting stents and Resolute Integrity durable polymer zotarolimus-eluting stents: results of the ORIENT trial, EuroIntervention 12 (13) (2017) 1623–1631, https://doi.org/10.4244/EIJ-D-16-00179.

[36] S. Deepthi, M. Nivedhitha Sundaram, J. Deepti Kadavan, R. Jayakumar, Layered chitosan-collagen hydrogel/aligned PLLA nanofiber construct for flexor tendon regeneration, Carbohydr. Polym. 153 (2016) 492–500, https://doi.org/10.1016/j.carbpol.2016.07.124.

[37] K. Szustakiewicz, B. Kryszak, P. Dzienny, B. Pozniak, M. Tikhomirov, V. Hoppe, P. Szymczyk-Ziolkowska, W. Tylus, M. Grzymajlo, A. Gadomska-Gajadhur, A.J. Antonczak, Cytotoxicity study of UV-Laser-Irradiated PLLA surfaces subjected to bio-ceramisation: a new way towards implant surface modification, Int. J. Mol. Sci. 22 (16) (2021), https://doi.org/10.3390/ijms22168436.

[38] S. Garg, P.W. Serruys, Coronary stents: looking forward, J. Am. Coll. Cardiol. 56 (10 Suppl) (2010) S43–S78, https://doi.org/10.1016/j.jacc.2010.06.008.

[39] S. Nishio, K. Kosuga, K. Igaki, M. Okada, E. Kyo, T. Tsuji, E. Takeuchi, Y. Inuzuka, S. Takeda, T. Hata, Y. Takeuchi, Y. Kawada, T. Harita, J. Seki, S. Akamatsu, S. Hasegawa, N. Bruining, S. Brugaletta, S. de Winter, T. Muramatsu, Y. Onuma, P.W. Serruys, S. Ikeguchi, Long-Term (>10 Years) clinical outcomes of first-in-human biodegradable poly-l-lactic acid coronary stents: Igaki-Tamai stents, Circulation 125 (19) (2012) 2343–2353, https://doi.org/10.1161/CIRCULATIONAHA.110.000901.

[40] J.A. Ormiston, P.W. Serruys, Y. Onuma, R.J. van Geuns, B. de Bruyne, D. Dudek, L. Thuesen, P.C. Smits, B. Chevalier, D. McClean, J. Koolen, S. Windecker, R. Whitbourn, I. Meredith, C. Dorange, S. Veldhof, K.M. Hebert, R. Rapoza, H.M. Garcia-Garcia, First serial assessment at 6 months and 2 years of the second generation of absorb everolimus-eluting bioresorbable vascular scaffold: a multi-imaging modality study, Circ. Cardiovasc. Interv. 5 (5) (2012) 620–632, https://doi.org/10.1161/CIRCINTERVENTIONS.112.971549.

[41] P.W. Serruys, Y. Onuma, H.M. Garcia-Garcia, T. Muramatsu, R.J. van Geuns, B. de Bruyne, D. Dudek, L. Thuesen, P.C. Smits, B. Chevalier, D. McClean, J. Koolen, S. Windecker, R. Whitbourn, I. Meredith, C. Dorange, S. Veldhof, K.M. Hebert, R. Rapoza, J.A. Ormiston, Dynamics of vessel wall changes following the implantation of the absorb everolimus-eluting bioresorbable vascular scaffold: a multi-imaging modality study at 6, 12, 24 and 36 months, EuroIntervention 9 (11) (2014) 1271–1284, https://doi.org/10.4244/EIJV9I11A217.

[42] E. Tenekecioglu, V. Farooq, C.V. Bourantas, R.C. Silva, Y. Onuma, M. Yilmaz, P.W. Serruys, Bioresorbable scaffolds: a new paradigm in percutaneous coronary intervention, BMC Cardiovasc. Disord. 16 (2016) 38, https://doi.org/10.1186/s12872-016-0207-5.

[43] A. Kumar, B.D. Gogas, E.W. Thompson, G.M. Burnett, D. Molony, H. Hosseini, K. Chandran, A. Lefieux, Y. Honda, J.M. Lee, P.W. Serruys, D.J. Kereiakes, G.W. Stone, H. Samady, Collaborators, Bioresorbable vascular scaffolds versus everolimus-eluting stents: a biomechanical analysis of the ABSORB III Imaging substudy, EuroIntervention 16 (12) (2020) e989–e996, https://doi.org/10.4244/EIJ-D-19-01128.

[44] J.J. Wykrzykowska, R.P. Kraak, S.H. Hofma, R.J. van der Schaaf, E.K. Arkenbout, I.J. Aj, J. Elias, I.M. van Dongen, R.Y.G. Tijssen, K.T. Koch, J. Baan Jr., M.M. Vis, R.J. de Winter, J.J. Piek, J.G.P. Tijssen, J.P.S. Henriques, A. Investigators, Bioresorbable scaffolds versus metallic stents in routine PCI, N. Engl. J. Med. 376 (24) (2017) 2319–2328, https://doi.org/10.1056/NEJMoa1614954.

[45] A. Abizaid, R.A. Costa, J. Schofer, J. Ormiston, M. Maeng, B. Witzenbichler, R.V. Botelho, J.R. Costa Jr., D. Chamie, A.S. Abizaid, J.P. Castro, L. Morrison, S. Toyloy, V. Bhat, J. Yan, S. Verheye, Serial multimodality imaging and 2-year clinical outcomes of the novel DESolve novolimus-eluting bioresorbable coronary scaffold system for the treatment of single de novo coronary lesions, JACC Cardiovasc. Interv. 9 (6) (2016) 565–574, https://doi.org/10.1016/j.jcin.2015.12.004.

[46] T.P. Vahl, P. Gasior, C.A. Gongora, K. Ramzipoor, C. Lee, Y. Cheng, J. McGregor, M. Shibuya, E.A. Estrada, G.B. Conditt, G.L. Kaluza, J.F. Granada, Four-year polymer biocompatibility and vascular healing profile of a novel ultrahigh molecular weight amorphous PLLA bioresorbable vascular scaffold: an OCT study in healthy porcine coronary arteries, EuroIntervention 12 (12) (2016) 1510–1518, https://doi.org/10.4244/EIJ-D-16-00308.

[47] Y. Wu, L. Shen, L. Ge, Q. Wang, J. Qian, F. Zhang, K. Yao, D. Huang, Y. Chen, J. Ge, Six-month outcomes of the XINSORB bioresorbable sirolimus-eluting scaffold in treating single de novo lesions in human coronary artery, Catheter Cardiovasc Interv. https://doi.org/10.1002/ccd.26404, 2016, 87-Suppl 1-630-637.

[48] R. Jabara, N. Chronos, K. Robinson, Novel bioabsorbable salicylate-based polymer as a drug-eluting stent coating, Cathet. Cardiovasc. Interv. 72 (2) (2008) 186–194, https://doi.org/10.1002/ccd.21607.

[49] J. Iqbal, Y. Onuma, J. Ormiston, A. Abizaid, R. Waksman, P. Serruys, Bioresorbable scaffolds: rationale, current status, challenges, and future, Eur. Heart J. 35 (12) (2014) 765–776, https://doi.org/10.1093/eurheartj/eht542.
[50] G. Acharya, C.H. Lee, Y. Lee, Optimization of cardiovascular stent against restenosis: factorial design-based statistical analysis of polymer coating conditions, PLoS One 7 (8) (2012), e43100, https://doi.org/10.1371/journal.pone.0043100.
[51] A. Biswas, A.P. Singh, D. Rana, V.K. Aswal, P. Maiti, Biodegradable toughened nanohybrid shape memory polymer for smart biomedical applications, Nanoscale 10 (21) (2018) 9917–9934, https://doi.org/10.1039/c8nr01438h.
[52] K. Polak-Krasna, A.R. Abaei, R.N. Shirazi, E. Parle, O. Carroll, W. Ronan, T.J. Vaughan, Physical and mechanical degradation behaviour of semi-crystalline PLLA for bioresorbable stent applications, J. Mech. Behav. Biomed. Mater. 118 (2021), 104409, https://doi.org/10.1016/j.jmbbm.2021.104409.
[53] D. Papkov, N. Delpouve, L. Delbreilh, S. Araujo, T. Stockdale, S. Mamedov, K. Maleckis, Y. Zou, M.N. Andalib, E. Dargent, V.P. Dravid, M.V. Holt, C. Pellerin, Y.A. Dzenis, Quantifying polymer chain orientation in strong and tough nanofibers with low crystallinity: toward next generation nanostructured superfibers, ACS Nano 13 (5) (2019) 4893–4927, https://doi.org/10.1021/acsnano.8b08725.
[54] H. Tamai, K. Igaki, E. Kyo, K. Kosuga, A. Kawashima, S. Matsui, H. Komori, T. Tsuji, S. Motohara, H. Uehata, Initial and 6-month results of biodegradable poly-l-lactic acid coronary stents in humans, Circulation 102 (4) (2000) 399–404, https://doi.org/10.1161/01.cir.102.4.399.
[55] A.K. Bledzki, J. Gassan, Composites reinforced with cellulose based fibres, Prog. Polym. Sci. 24 (2) (1999) 221–274, https://doi.org/Doi 10.1016/S0079-6700(98)00018-5.
[56] S.J. Eichhorn, C.A. Baillie, N. Zafeiropoulos, L.Y. Mwaikambo, M.P. Ansell, A. Dufresne, K.M. Entwistle, P.J. Herrera-Franco, G.C. Escamilla, L. Groom, M. Hughes, C. Hill, T.G. Rials, P.M. Wild, Review: current international research into cellulosic fibres and composites, J. Mater. Sci. 36 (9) (2001) 2107–2131, https://doi.org/Doi 10.1023/A:1017512029696.
[57] T. Zimmermann, E. Poehler, T. Geiger, Cellulose fibrils for polymer reinforcement, Abstr. Pap. Am. Chem. Soc. 229 (2005), U313. U313.
[58] Q. Wang, G. Fang, Y. Zhao, G. Wang, T. Cai, Computational and experimental investigation into mechanical performances of Poly-L-Lactide Acid (PLLA) coronary stents, J. Mech. Behav. Biomed. Mater. 65 (2017) 415–427, https://doi.org/10.1016/j.jmbbm.2016.08.033.
[59] S.-Y. Gu, K. Chang, S.-P. Jin, A dual-induced self-expandable stent based on biodegradable shape memory polyurethane nanocomposites (PCLAU/Fe3 O4) triggered around body temperature, J. Appl. Polym. Sci. 135 (3) (2018), https://doi.org/10.1002/app.45686.
[60] K. Omagari, K. Ueda, Z. Zhijing, K. Higashi, M. Inoue, T. Fukami, K. Moribe, Mechanistic study of preparation of drug/polymer/surfactant ternary hot extrudates to obtain small and stable drug nanocrystal suspensions, Int. J. Pharm. 591 (2020), 120003, https://doi.org/10.1016/j.ijpharm.2020.120003.
[61] S. Cong, A. Creamer, Z. Fei, S.A.J. Hillman, C. Rapley, J. Nelson, M. Heeney, Tunable control of the hydrophilicity and wettability of conjugated polymers by a postpolymerization modification approach, Macromol. Biosci. 20 (11) (2020), e2000087, https://doi.org/10.1002/mabi.202000087.
[62] L. Bekale, D. Agudelo, H.A. Tajmir-Riahi, Effect of polymer molecular weight on chitosan-protein interaction, Colloids Surf. B Biointerfaces 125 (2015) 309–317, https://doi.org/10.1016/j.colsurfb.2014.11.037.
[63] M. Behl, A. Lendlein, Actively moving polymers, Soft Matter 3 (1) (2006) 58–67, https://doi.org/10.1039/b610611k.
[64] H. Jia, S.Y. Gu, K. Chang, 3D printed self-expandable vascular stents from biodegradable shape memory polymer, Adv. Polym. Technol. 37 (8) (2018) 3222–3228, https://doi.org/10.1002/adv.22091.
[65] G.I. Peterson, A.V. Dobrynin, M.L. Becker, Biodegradable shape memory polymers in medicine, Adv. Healthc. Mater. 6 (21) (2017), https://doi.org/10.1002/adhm.201700694.
[66] W. Zhao, L. Liu, F. Zhang, J. Leng, Y. Liu, Shape memory polymers and their composites in biomedical applications, Mater Sci Eng C Mater Biol Appl 97 (2019) 864–883, https://doi.org/10.1016/j.msec.2018.12.054.
[67] S.H. Ajili, N.G. Ebrahimi, M. Soleimani, Polyurethane/polycaprolactane blend with shape memory effect as a proposed material for cardiovascular implants, Acta Biomater. 5 (5) (2009) 1519–1530, https://doi.org/10.1016/j.actbio.2008.12.014.
[68] L.S. Nair, C.T. Laurencin, Biodegradable polymers as biomaterials, Prog. Polym. Sci. 32 (8–9) (2007) 762–798, https://doi.org/10.1016/j.progpolymsci.2007.05.017.
[69] S.S. Venkatraman, L.P. Tan, J.F. Joso, Y.C. Boey, X. Wang, Biodegradable stents with elastic memory, Biomaterials 27 (8) (2006) 1573–1578, https://doi.org/10.1016/j.biomaterials.2005.09.002.
[70] R. Duarah, Y.P. Singh, P. Gupta, B.B. Mandal, N. Karak, High performance bio-based hyperbranched polyurethane/carbon dot-silver nanocomposite: a rapid self-expandable stent, Biofabrication 8 (4) (2016), 045013, https://doi.org/10.1088/1758-5090/8/4/045013.
[71] J. Dominguez-Robles, T.J. Shen, V.A. Cornelius, F. Corduas, E. Mancuso, R.F. Donnelly, A. Margariti, D.A. Lamprou, E. Larraneta, Development of drug loaded cardiovascular prosthesis for thrombosis prevention using 3D printing, Mater. Sci. Eng. C-Mater. 129 (2021) https://doi.org/ARTN 112375 10.1016/j.msec.2021.112375.
[72] R. van Lith, E. Baker, H. Ware, J. Yang, A.C. Farsheed, C. Sun, G. Ameer, 3D-Printing strong high-resolution antioxidant bioresorbable vascular stents, Adv. Mater. Technol.-Us 1 (9) (2016) https://doi.org/ARTN 1600138 10.1002/admt.201600138.
[73] S. Garg, P.W. Serruys, Coronary stents current status, J. Am. Coll. Cardiol. 56 (10) (2010) S1–S42, https://doi.org/10.1016/j.jacc.2010.06.007.
[74] N. Sandler, M. Preis, Printed drug-delivery systems for improved patient treatment, Trends Pharmacol. Sci. 37 (12) (2016) 1070–1080, https://doi.org/10.1016/j.tips.2016.10.002.
[75] A. Shafiee, A. Atala, Printing technologies for medical applications, Trends Mol. Med. 22 (3) (2016) 254–265, https://doi.org/10.1016/j.molmed.2016.01.003.
[76] T. Yin, R. Du, Y. Wang, J. Huang, S. Ge, Y. Huang, Y. Tan, Q. Liu, Z. Chen, H. Feng, J. Du, Y. Wang, G. Wang, Two-stage degradation and novel functional endothelium characteristics of a 3-D printed bioresorbable scaffold, Bioact. Mater. 10 (2022) 378–396, https://doi.org/10.1016/j.bioactmat.2021.08.020.
[77] C. Zhang, H. Deng, S.M. Kenderes, J.W. Su, A.G. Whittington, J. Lin, Chemically interconnected thermotropic polymers for transparency-tunable and impact-resistant windows, Acs Appl. Mater. Inter. 11 (5) (2019) 5393–5400, https://doi.org/10.1021/acsami.8b19740.
[78] Y. Li, C.X. Ji, L.H. Mei, J.W. Qiang, S. Ju, Oral administration of trace element magnesium significantly improving the cognition and locomotion in hepatic encephalopathy rats, Sci. Rep. 7 (1) (2017) 1817, https://doi.org/10.1038/s41598-017-02101-8.
[79] Z.Q. Zhang, Y.X. Yang, J.A. Li, R.C. Zeng, S.K. Guan, Advances in coatings on magnesium alloys for cardiovascular stents - a review, Bioact. Mater. 6 (12) (2021) 4729–4757, https://doi.org/10.1016/j.bioactmat.2021.04.044.
[80] B. Heublein, R. Rohde, V. Kaese, M. Niemeyer, W. Hartung, A. Haverich, Biocorrosion of magnesium alloys: a new principle in cardiovascular implant technology? Heart 89 (6) (2003) 651–656, https://doi.org/10.1136/heart.89.6.651.
[81] D. Zhao, F. Witte, F. Lu, J. Wang, J. Li, L. Qin, Current status on clinical applications of magnesium-based orthopaedic implants: a review from clinical translational perspective, Biomaterials 112 (2017) 287–302, https://doi.org/10.1016/j.biomaterials.2016.10.017.
[82] P. Erne, M. Schier, T.J. Resink, The road to bioabsorbable stents: reaching clinical reality? Cardiovasc. Intervent. Radiol. 29 (1) (2006) 11–16, https://doi.org/10.1007/s00270-004-0341-9.
[83] J. Yang, F. Cui, I.S. Lee, Surface modifications of magnesium alloys for biomedical applications, Ann. Biomed. Eng. 39 (7) (2011) 1857–1871, https://doi.org/10.1007/s10439-011-0300-y.
[84] P.K. Bowen, A. Drelich, J. Drelich, J. Goldman, Rates of in vivo (arterial) and in vitro biocorrosion for pure magnesium, J. Biomed. Mater. Res. 103 (1) (2015) 341–349, https://doi.org/10.1002/jbm.a.35179.
[85] M.S. Uddin, C. Hall, P. Murphy, Surface treatments for controlling corrosion rate of biodegradable Mg and Mg-based alloy implants, Sci. Technol. Adv. Mater. 16 (5) (2015), 053501, https://doi.org/10.1088/1468-6996/16/5/053501.
[86] Y. Liu, S. Li, Y. Wang, H. Wang, K. Gao, Z. Han, L. Ren, Superhydrophobic and superoleophobic surface by electrodeposition on magnesium alloy substrate: wettability and corrosion inhibition, J. Colloid Interface Sci. 478 (2016) 164–171, https://doi.org/10.1016/j.jcis.2016.06.006.
[87] J. Ma, N. Zhao, L. Betts, D. Zhu, Bio-adaption between magnesium alloy stent and the blood vessel: a review, J. Mater. Sci. Technol. 32 (9) (2016) 815–826, https://doi.org/10.1016/j.jmst.2015.12.018.
[88] P. Peeters, M. Bosiers, J. Verbist, K. Deloose, B. Heublein, Preliminary results after application of absorbable metal stents in patients with critical limb ischemia, J. Endovasc. Ther. 12 (1) (2005) 1–5, https://doi.org/10.1583/04-1349R.1.
[89] M. Bosiers, K. Deloose, J. Verbist, P. Peeters, First clinical application of absorbable metal stents in the treatment of critical limb ischemia: 12-month results, Vasc. Dis. Manag. 2 (4) (2005) 86–91.
[90] M. Bosiers, P. Peeters, O. D'Archambeau, J. Hendriks, E. Pilger, C. Duber, T. Zeller, A. Gussmann, P.N. Lohle, E. Minar, D. Scheinert, K. Hausegger, K.L. Schulte, J. Verbist, K. Deloose, J. Lammer, A.I. Investigators, AMS INSIGHT–absorbable metal stent implantation for treatment of below-the-knee critical limb ischemia: 6-month analysis, Cardiovasc. Intervent. Radiol. 32 (3) (2009) 424–435, https://doi.org/10.1007/s00270-008-9472-8.
[91] R. Erbel, C. Di Mario, J. Bartunek, J. Bonnier, B. de Bruyne, F.R. Eberli, P. Erne, M. Haude, B. Heublein, M. Horrigan, C. Ilsley, D. Bose, J. Koolen, T.F. Luscher, N. Weissman, R. Waksman, P.-A. Investigators, Temporary scaffolding of coronary arteries with bioabsorbable magnesium stents: a prospective, non-randomised multicentre trial, Lancet 369 (9576) (2007) 1869–1875, https://doi.org/10.1016/S0140-6736(07)60853-8.
[92] J.M. Lasala, D.A. Cox, D. Dobies, K. Baran, W.B. Bachinsky, E.W. Rogers, J.A. Breall, D.H. Lewis, A. Song, R.M. Starzyk, S.R. Mascioli, K.D. Dawkins, D.S. Baim, Arrive, A.P. Physicians, Drug-eluting stent thrombosis in routine clinical practice: two-year outcomes and predictors from the TAXUS ARRIVE registries, Circ. Cardiovasc. Interv. 2 (4) (2009) 285–293, https://doi.org/10.1161/CIRCINTERVENTIONS.109.852178.109.852178.
[93] M. Haude, R. Erbel, P. Erne, S. Verheye, H. Degen, D. Bose, P. Vermeersch, I. Wijnbergen, N. Weissman, F. Prati, R. Waksman, J. Koolen, Safety and performance of the drug-eluting absorbable metal scaffold (DREAMS) in patients with de-novo coronary lesions: 12 month results of the prospective, multicentre, first-in-man BIOSOLVE-I trial, Lancet 381 (9869) (2013) 836–844, https://doi.org/10.1016/S0140-6736(12)61765-6.
[94] M. Haude, R. Erbel, P. Erne, S. Verheye, H. Degen, P. Vermeersch, N. Weissman, F. Prati, N. Bruining, R. Waksman, J. Koolen, Safety and performance of the DRug-Eluting Absorbable Metal Scaffold (DREAMS) in patients with de novo coronary lesions: 3-year results of the prospective, multicentre, first-in-man BIOSOLVE-I trial, EuroIntervention 12 (2) (2016) e160–166, https://doi.org/10.4244/EIJ-D-15-00371.

[95] M. Haude, H. Ince, A. Abizaid, R. Toelg, P.A. Lemos, C. von Birgelen, E.H. Christiansen, W. Wijns, F.J. Neumann, C. Kaiser, E. Eeckhout, S.T. Lim, J. Escaned, H.M. Garcia-Garcia, R. Waksman, Safety and performance of the second-generation drug-eluting absorbable metal scaffold in patients with de-novo coronary artery lesions (BIOSOLVE-II): 6 month results of a prospective, multicentre, non-randomised, first-in-man trial, Lancet 387 (10013) (2016) 31–39, https://doi.org/10.1016/S0140-6736(15)00447-X.

[96] M. Haude, H. Ince, A. Abizaid, R. Toelg, P.A. Lemos, C. von Birgelen, E.H. Christiansen, W. Wijns, F.J. Neumann, C. Kaiser, E. Eeckhout, S.T. Lim, J. Escaned, Y. Onuma, H.M. Garcia-Garcia, R. Waksman, Sustained safety and performance of the second-generation drug-eluting absorbable metal scaffold in patients with de novo coronary lesions: 12-month clinical results and angiographic findings of the BIOSOLVE-II first-in-man trial, Eur. Heart J. 37 (35) (2016) 2701–2709, https://doi.org/10.1093/eurheartj/ehw196.

[97] H.M. Garcia-Garcia, M. Haude, K. Kuku, A. Hideo-Kajita, H. Ince, A. Abizaid, R. Tolg, P.A. Lemos, C. von Birgelen, E.H. Christiansen, W. Wijns, J. Escaned, J. Dijkstra, R. Waksman, In vivo serial invasive imaging of the second-generation drug-eluting absorbable metal scaffold (Magmaris - DREAMS 2G) in de novo coronary lesions: insights from the BIOSOLVE-II First-In-Man Trial, Int. J. Cardiol. 255 (2018) 22–28, https://doi.org/10.1016/j.ijcard.2017.12.053.

[98] M. Haude, H. Ince, R. Toelg, P.A. Lemos, C. von Birgelen, E.H. Christiansen, W. Wijns, F.J. Neumann, E. Eeckhout, H.M. Garcia-Garcia, R. Waksman, Safety and performance of the second-generation drug-eluting absorbable metal scaffold (DREAMS 2G) in patients with de novo coronary lesions: three-year clinical results and angiographic findings of the BIOSOLVE-II first-in-man trial, EuroIntervention 15 (15) (2020) e1375–e1382, https://doi.org/10.4244/EIJ-D-18-01000.

[99] M. Haude, H. Ince, S. Kische, A. Abizaid, R. Tolg, P. Alves Lemos, N.M. Van Mieghem, S. Verheye, C. von Birgelen, E.H. Christiansen, E. Barbato, H.M. Garcia-Garcia, R. Waksman, Biosolve II, I.I.I. investigators, Safety and clinical performance of a drug eluting absorbable metal scaffold in the treatment of subjects with de novo lesions in native coronary arteries: pooled 12-month outcomes of BIOSOLVE-II and BIOSOLVE-III, Cathet. Cardiovasc. Interv. 92 (7) (2018) E502–E511, https://doi.org/10.1002/ccd.27680.

[100] M. Haude, H. Ince, S. Kische, A. Abizaid, R. Tolg, P. Alves Lemos, N.M. Van Mieghem, S. Verheye, C. von Birgelen, E.H. Christiansen, W. Wijns, H.M. Garcia-Garcia, R. Waksman, Sustained safety and clinical performance of a drug-eluting absorbable metal scaffold up to 24 months: pooled outcomes of BIOSOLVE-II and BIOSOLVE-III, EuroIntervention 13 (4) (2017) 432–439, https://doi.org/10.4244/EIJ-D-17-00254.

[101] A. Hideo-Kajita, H.M. Garcia-Garcia, P. Kolm, V. Azizi, Y. Ozaki, K. Dan, H. Ince, S. Kische, A. Abizaid, R. Toelg, P.A. Lemos, N.M. Van Mieghem, S. Verheye, C. von Birgelen, E.H. Christiansen, W. Wijns, T. Lefevre, S. Windecker, R. Waksman, M. Haude, B. Bioflow-Ii, B.-I. investigators, Comparison of clinical outcomes between Magmaris and Orsiro drug eluting stent at 12months: pooled patient level analysis from BIOSOLVE II-III and BIOFLOW II trials, II, Int. J. Cardiol. 300 (2020) 60–65, https://doi.org/10.1016/j.ijcard.2019.11.003.

[102] M. Haude, H. Ince, S. Kische, R. Toelg, N.M. Van Mieghem, S. Verheye, C. von Birgelen, E.H. Christiansen, E. Barbato, H.M. Garcia-Garcia, R. Waksman, Sustained safety and performance of the second-generation sirolimus-eluting absorbable metal scaffold: pooled outcomes of the BIOSOLVE-II and -iii trials at 3 years, Cardiovasc. Revascularization Med. 21 (9) (2020) 1150–1154, https://doi.org/10.1016/j.carrev.2020.04.006.

[103] Q. de Hemptinne, F. Picard, R. Briki, A. Awada, P.G. Silance, D. Dolatabadi, N. Debbas, P. Unger, Drug-eluting resorbable magnesium scaffold implantation in ST-segment elevation myocardial infarction: a pilot study, J. Invasive Cardiol. 30 (6) (2018) 202–206.

[104] M. Sabate, F. Alfonso, A. Cequier, S. Romani, P. Bordes, A. Serra, A. Iniguez, P. Salinas, B. Garcia Del Blanco, J. Goicolea, R. Hernandez-Antolin, J. Cuesta, J.A. Gomez-Hospital, L. Ortega-Paz, J. Gomez-Lara, S. Brugaletta, Magnesium-based resorbable scaffold versus permanent metallic sirolimus-eluting stent in patients with ST-segment elevation myocardial infarction: the MAGSTEMI randomized clinical trial, Circulation 140 (23) (2019) 1904–1916, https://doi.org/10.1161/CIRCULATIONAHA.119.043467.

[105] S. Verheye, A. Wlodarczak, P. Montorsi, J. Torzewski, J. Bennett, M. Haude, G. Starmer, T. Buck, M. Wiemer, A.A.B. Nuruddin, B.P. Yan, M.K. Lee, BIOSOLVE-IV-registry: safety and performance of the Magmaris scaffold: 12-month outcomes of the first cohort of 1,075 patients, Cathet. Cardiovasc. Interv. 98 (1) (2021) E1–E8, https://doi.org/10.1002/ccd.29260.

[106] E. Cerrato, U. Barbero, J.A. Gil Romero, G. Quadri, H. Mejia-Renteria, F. Tomassini, F. Ferrari, F. Varbella, N. Gonzalo, J. Escaned, Magmaris resorbable magnesium scaffold: state-of-art review, Future Cardiol. 15 (4) (2019) 267–279, https://doi.org/10.2217/fca-2018-0081.

[107] Z.-Y. Ding, L.-Y. Cui, R.-C. Zeng, Y.-B. Zhao, S.-K. Guan, D.-K. Xu, C.-G. Lin, Exfoliation corrosion of extruded Mg-Li-Ca alloy, J. Mater. Sci. Technol. 34 (9) (2018) 1550–1557, https://doi.org/10.1016/j.jmst.2018.05.014.

[108] K. Harawaza, B. Cousins, P. Roach, A. Fernandez, Modification of the surface nanotopography of implant devices: a translational perspective, Mater. Today Biol. 12 (2021), 100152, https://doi.org/10.1016/j.mtbio.2021.100152.

[109] H.X. Wang, S.K. Guan, X. Wang, C.X. Ren, L.G. Wang, In vitro degradation and mechanical integrity of Mg-Zn-Ca alloy coated with Ca-deficient hydroxyapatite by the pulse electrodeposition process, Acta Biomater. 6 (5) (2010) 1743–1748, https://doi.org/10.1016/j.actbio.2009.12.009.

[110] S.-M. Baek, S.-Y. Lee, J.C. Kim, J. Kwon, H. Jung, S. Lee, K.-S. Lee, S.S. Park, Role of trace additions of Mn and Y in improving the corrosion resistance of Mg–3Al–1Zn alloy, Corrosion Sci. 178 (2021), https://doi.org/10.1016/j.corsci.2020.108998.

[111] S.L. Zhou, W. Liu, S.C. Fu, Constitutive modelling of LZ91 magnesium-lithium alloy sheet by uniaxial tension loading tests, Mater. Today Proc. 33 (2020) 1787–1791, https://doi.org/10.1016/j.matpr.2020.05.052.

[112] D. Bian, X. Zhou, J. Liu, W. Li, D. Shen, Y. Zheng, W. Gu, J. Jiang, M. Li, X. Chu, L. Ma, X. Wang, Y. Zhang, S. Leeflang, J. Zhou, Degradation behaviors and in-vivo biocompatibility of a rare earth- and aluminum-free magnesium-based stent, Acta Biomater. 124 (2021) 382–397, https://doi.org/10.1016/j.actbio.2021.01.031.

[113] Y. Yue, L. Wang, N. Yang, J. Huang, L. Lei, H. Ye, L. Ren, S. Yang, Effectiveness of biodegradable magnesium alloy stents in coronary artery and femoral artery, J. Intervent. Cardiol. 28 (4) (2015) 358–364, https://doi.org/10.1111/joic.12217.

[114] W. Ding, Opportunities and challenges for the biodegradable magnesium alloys as next-generation biomaterials, Regen. Biomater. 3 (2) (2016) 79–86, https://doi.org/10.1093/rb/rbw003.

[115] J. Zhu, X. Zhang, J. Niu, Y. Shi, Z. Zhu, D. Dai, C. Chen, J. Pei, G. Yuan, R. Zhang, Biosafety and efficacy evaluation of a biodegradable magnesium-based drug-eluting stent in porcine coronary artery, Sci. Rep. 11 (1) (2021) 7330, https://doi.org/10.1038/s41598-021-86803-0.

[116] Z. Li, X. Gu, S. Lou, Y. Zheng, The development of binary Mg-Ca alloys for use as biodegradable materials within bone, Biomaterials 29 (10) (2008) 1329–1344, https://doi.org/10.1016/j.biomaterials.2007.12.021.

[117] W. Wang, H. Wu, R. Zan, Y. Sun, C. Blawert, S. Zhang, J. Ni, M.L. Zheludkevich, X. Zhang, Microstructure controls the corrosion behavior of a lean biodegradable Mg-2Zn alloy, Acta Biomater. 107 (2020) 349–361, https://doi.org/10.1016/j.actbio.2020.02.040.

[118] S. Liu, H. Guo, Balling behavior of selective laser melting (SLM) magnesium alloy, Materials 13 (16) (2020), https://doi.org/10.3390/ma13163632.

[119] Y. Qin, P. Wen, H. Guo, D. Xia, Y. Zheng, L. Jauer, R. Poprawe, M. Voshage, J.H. Schleifenbaum, Additive manufacturing of biodegradable metals: current research status and future perspectives, Acta Biomater. 98 (2019) 3–22, https://doi.org/10.1016/j.actbio.2019.04.046.

[120] C. Chen, J. Chen, W. Wu, Y. Shi, L. Jin, L. Petrini, L. Shen, G. Yuan, W. Ding, J. Ge, E.R. Edelman, F. Migliavacca, In vivo and in vitro evaluation of a biodegradable magnesium vascular stent designed by shape optimization strategy, Biomaterials 221 (2019), 119414, https://doi.org/10.1016/j.biomaterials.2019.119414.

[121] L. Mikhalovska, N. Chorna, O. Lazarenko, P. Haworth, A. Sudre, S. Mikhalovsky, Inorganic coatings for cardiovascular stents: in vitro and in vivo studies, J. Biomed. Mater. Res. B Appl. Biomater. 96 (2) (2011) 333–341, https://doi.org/10.1002/jbm.b.31772.

[122] Z. Wei, P. Tian, X. Liu, B. Zhou, Hemocompatibility and selective cell fate of polydopamine-assisted heparinized PEO/PLLA composite coating on biodegradable AZ31 alloy, Colloids Surf. B Biointerfaces 121 (2014) 451–460, https://doi.org/10.1016/j.colsurfb.2014.06.036.

[123] M. Echeverry-Rendon, F. Echeverria, M.C. Harmsen, Interaction of different cell types with magnesium modified by plasma electrolytic oxidation, Colloids Surf. B Biointerfaces 193 (2020), 111153, https://doi.org/10.1016/j.colsurfb.2020.111153.

[124] F. Peng, D. Wang, Y. Tian, H. Cao, Y. Qiao, X. Liu, Sealing the pores of PEO coating with Mg-Al layered double hydroxide: enhanced corrosion resistance, cytocompatibility and drug delivery ability, Sci. Rep. 7 (1) (2017) 8167, https://doi.org/10.1038/s41598-017-08238-w.

[125] F. Peng, H. Li, D. Wang, P. Tian, Y. Tian, G. Yuan, D. Xu, X. Liu, Enhanced corrosion resistance and biocompatibility of magnesium alloy by Mg-Al-layered double hydroxide, ACS Appl. Mater. Interfaces 8 (51) (2016) 35033–35044, https://doi.org/10.1021/acsami.6b12974.

[126] Y. Ren, P. Sikder, B. Lin, S.B. Bhaduri, Microwave assisted coating of bioactive amorphous magnesium phosphate (AMP) on polyetheretherketone (PEEK), Mater Sci Eng C Mater Biol Appl 85 (2018) 107–113, https://doi.org/10.1016/j.msec.2017.12.025.

[127] J. Sun, Y. Zhu, L. Meng, P. Chen, T. Shi, X. Liu, Y. Zheng, Electrophoretic deposition of colloidal particles on Mg with cytocompatibility, antibacterial performance, and corrosion resistance, Acta Biomater. 45 (2016) 387–398, https://doi.org/10.1016/j.actbio.2016.09.007.

[128] K. Jelonek, J. Jaworska, M. Pastusiak, M. Sobota, J. Wlodarczyk, P. Karpeta-Jarzabek, B. Kaczmarczyk, J. Kasperczyk, P. Dobrzynski, Effect of vascular scaffold composition on release of sirolimus, Eur. J. Pharm. Biopharm. 132 (2018) 41–49, https://doi.org/10.1016/j.ejpb.2018.08.015.

[129] C.Y. Li, L. Gao, X.L. Fan, R.C. Zeng, D.C. Chen, K.Q. Zhi, In vitro degradation and cytocompatibility of a low temperature in-situ grown self-healing Mg-Al LDH coating on MAO-coated magnesium alloy AZ31, Bioact. Mater. 5 (2) (2020) 364–376, https://doi.org/10.1016/j.bioactmat.2020.02.008.

[130] X. He, G. Zhang, Y. Pei, H. Zhang, Layered hydroxide/polydopamine/hyaluronic acid functionalized magnesium alloys for enhanced anticorrosion, biocompatibility and antithrombogenicity in vascular stents, J. Biomater. Appl. 34 (8) (2020) 1131–1141, https://doi.org/10.1177/0885328219899233.

[131] R. Kanwar, M. Gradzielski, S. Prevost, G. Kaur, M.S. Appavou, S.K. Mehta, Physicochemical stimuli as tuning parameters to modulate the structure and stability of nanostructured lipid carriers and release kinetics of encapsulated antileprosy drugs, J. Mater. Chem. B 7 (42) (2019) 6539–6555, https://doi.org/10.1039/c9tb01330j.

[132] H. Li, F. Peng, D. Wang, Y. Qiao, D. Xu, X. Liu, Layered double hydroxide/polydopamine composite coating with surface heparinization on Mg alloys: improved anticorrosion, endothelialization and hemocompatibility, Biomater. Sci. 6 (7) (2018) 1846–1858, https://doi.org/10.1039/c8bm00298c.

[133] H.J. Yu, J.Q. Wang, X.T. Shi, D.V. Louzguine-Luzgin, H.K. Wu, J.H. Perepezko, Ductile biodegradable Mg-based metallic glasses with excellent biocompatibility,

Adv. Funct. Mater. 23 (38) (2013) 4793–4800, https://doi.org/10.1002/adfm.201203738.
[134] Y.F. Zhou, P.C. Li, J.H. Wu, J.A. Haslam, L. Mao, Y.P. Xia, Q.W. He, X.X. Wang, H. Lei, X.L. Lan, Q.R. Miao, Z.Y. Yue, Y.N. Li, B. Hu, Sema3E/PlexinD1 inhibition is a therapeutic strategy for improving cerebral perfusion and restoring functional loss after stroke in aged rats, Neurobiol. Aging 70 (2018) 102–116, https://doi.org/10.1016/j.neurobiolaging.2018.06.003.
[135] J.M. Seitz, M. Durisin, J. Goldman, J.W. Drelich, Recent advances in biodegradable metals for medical sutures: a critical review, Adv. Healthc. Mater. 4 (13) (2015) 1915–1936, https://doi.org/10.1002/adhm.201500189.
[136] S. Loffredo, C. Paternoster, N. Giguere, G. Barucca, M. Vedani, D. Mantovani, The addition of silver affects the deformation mechanism of a twinning-induced plasticity steel: potential for thinner degradable stents, Acta Biomater. 98 (2019) 103–113, https://doi.org/10.1016/j.actbio.2019.04.030.
[137] E. Scarcello, I. Lobysheva, C. Bouzin, P.J. Jacques, D. Lison, C. Dessy, Endothelial dysfunction induced by hydroxyl radicals - the hidden face of biodegradable Fe-based materials for coronary stents, Mater Sci Eng C Mater Biol Appl 112 (2020), 110938, https://doi.org/10.1016/j.msec.2020.110938.
[138] D. Zhang, Z. Cai, N. Liao, S. Lan, M. Wu, H. Sun, Z. Wei, J. Li, X. Liu, pH/hypoxia programmable triggered cancer photo-chemotherapy based on a semiconducting polymer dot hybridized mesoporous silica framework, Chem. Sci. 9 (37) (2018) 7390–7399, https://doi.org/10.1039/c8sc02408a.
[139] S.T. Chou, M. Alsawas, R.M. Fasano, J.J. Field, J.E. Hendrickson, J. Howard, M. Kameka, J.L. Kwiatkowski, F. Pirenne, P.A. Shi, S.R. Stowell, S.L. Thein, C.M. Westhoff, T.E. Wong, E.A. Akl, American Society of Hematology 2020 guidelines for sickle cell disease: transfusion support, Blood Adv. 4 (2) (2020) 327–355, https://doi.org/10.1182/bloodadvances.2019001143.
[140] P.P. Mueller, T. May, A. Perz, H. Hauser, M. Peuster, Control of smooth muscle cell proliferation by ferrous iron, Biomaterials 27 (10) (2006) 2193–2200, https://doi.org/10.1016/j.biomaterials.2005.10.042.
[141] B. Liu, Y.F. Zheng, Effects of alloying elements (Mn, Co, Al, W, Sn, B, C and S) on biodegradability and in vitro biocompatibility of pure iron, Acta Biomater. 7 (3) (2011) 1407–1420, https://doi.org/10.1016/j.actbio.2010.11.001.
[142] N.S. Fagali, M.A. Madrid, B.T. Perez Maceda, M.E. Lopez Fernandez, R.M. Lozano Puerto, M. Fernandez Lorenzo de Mele, Effect of degradation products of iron-bioresorbable implants on the physiological behavior of macrophages in vitro, Metallomics 12 (11) (2020) 1841–1850, https://doi.org/10.1039/d0mt00151a.
[143] W. Lin, L. Qin, H. Qi, D. Zhang, G. Zhang, R. Gao, H. Qiu, Y. Xia, P. Cao, X. Wang, W. Zheng, Long-term in vivo corrosion behavior, biocompatibility and bioresorption mechanism of a bioresorbable nitrided iron scaffold, Acta Biomater. 54 (2017) 454–468, https://doi.org/10.1016/j.actbio.2017.03.020.
[144] D. Bian, L. Qin, W. Lin, D. Shen, H. Qi, X. Shi, G. Zhang, H. Liu, H. Yang, J. Wang, D. Zhang, Y. Zheng, Magnetic resonance (MR) safety and compatibility of a novel iron bioresorbable scaffold, Bioact. Mater. 5 (2) (2020) 260–274, https://doi.org/10.1016/j.bioactmat.2020.02.011.
[145] Y. Qi, X. Li, Y. He, D. Zhang, J. Ding, Mechanism of acceleration of iron corrosion by a polylactide coating, ACS Appl. Mater. Interfaces 11 (1) (2019) 202–218, https://doi.org/10.1021/acsami.8b17125.
[146] Z. Wang, B. Yang, X. Chen, Q. Zhou, H. Li, S. Chen, D. Yin, H. He, M. He, Nobiletin regulates ROS/ADMA/DDAHII/eNOS/NO pathway and alleviates vascular endothelium injury by iron overload, Biol. Trace Elem. Res. 198 (1) (2020) 87–97, https://doi.org/10.1007/s12011-020-02038-6.
[147] X. Chen, H. Li, Z. Wang, Q. Zhou, S. Chen, B. Yang, D. Yin, H. He, M. He, Quercetin protects the vascular endothelium against iron overload damages via ROS/ADMA/DDAH/eNOS/NO pathway, Eur. J. Pharmacol. 868 (2020), 172885, https://doi.org/10.1016/j.ejphar.2019.172885.
[148] Q. Lu, V.A. Harris, R. Rafikov, X. Sun, S. Kumar, S.M. Black, Nitric oxide induces hypoxia ischemic injury in the neonatal brain via the disruption of neuronal iron metabolism, Redox Biol. 6 (2015) 112–121, https://doi.org/10.1016/j.redox.2015.06.007.
[149] G. Nair, S. Dodd, S.K. Ha, A.P. Koretsky, D.S. Reich, Ex vivo MR microscopy of a human brain with multiple sclerosis: visualizing individual cells in tissue using intrinsic iron, Neuroimage 223 (2020), 117285, https://doi.org/10.1016/j.neuroimage.2020.117285.
[150] T. Ganz, Macrophages and iron metabolism, Microbiol. Spectr. 4 (5) (2016), https://doi.org/10.1128/microbiolspec.MCHD-0037-2016.
[151] H.R. Cho, S.H. Choi, N. Lee, T. Hyeon, H. Kim, W.K. Moon, Macrophages homing to metastatic lymph nodes can be monitored with ultrasensitive ferromagnetic iron-oxide nanocubes and a 1.5T clinical MR scanner, PLoS One 7 (1) (2012), e29575, https://doi.org/10.1371/journal.pone.0029575.
[152] T. Huang, J. Cheng, Y.F. Zheng, In vitro degradation and biocompatibility of Fe-Pd and Fe-Pt composites fabricated by spark plasma sintering, Mater Sci Eng C Mater Biol Appl 35 (2014) 43–53, https://doi.org/10.1016/j.msec.2013.10.023.
[153] J. Capek, J. Kubasek, D. Vojtech, E. Jablonska, J. Lipov, T. Ruml, Microstructural, mechanical, corrosion and cytotoxicity characterization of the hot forged FeMn30(wt.%) alloy, Mater Sci Eng C Mater Biol Appl 58 (2016) 900–908, https://doi.org/10.1016/j.msec.2015.09.049.
[154] H. Hermawan, D. Mantovani, Process of prototyping coronary stents from biodegradable Fe-Mn alloys, Acta Biomater. 9 (10) (2013) 8585–8592, https://doi.org/10.1016/j.actbio.2013.04.027.
[155] A. Francis, Y. Yang, S. Virtanen, A.R. Boccaccini, Iron and iron-based alloys for temporary cardiovascular applications, J. Mater. Sci. Mater. Med. 26 (3) (2015) 138, https://doi.org/10.1007/s10856-015-5473-8.
[156] U. Allenstein, Y. Ma, A. Arabi-Hashemi, M. Zink, S.G. Mayr, Fe-Pd based ferromagnetic shape memory actuators for medical applications: biocompatibility, effect of surface roughness and protein coatings, Acta Biomater. 9 (3) (2013) 5845–5853, https://doi.org/10.1016/j.actbio.2012.10.040.
[157] T. Huang, Y. Cheng, Y. Zheng, In vitro studies on silver implanted pure iron by metal vapor vacuum arc technique, Colloids Surf. B Biointerfaces 142 (2016) 20–29, https://doi.org/10.1016/j.colsurfb.2016.01.065.
[158] W. Lin, G. Zhang, P. Cao, D. Zhang, Y. Zheng, R. Wu, L. Qin, G. Wang, T. Wen, Cytotoxicity and its test methodology for a bioabsorbable nitrided iron stent, J. Biomed. Mater. Res. B Appl. Biomater. 103 (4) (2015) 764–776, https://doi.org/10.1002/jbm.b.33246.
[159] D. Sarkar, J.A. Ankrum, G.S. Teo, C.V. Carman, J.M. Karp, Cellular and extracellular programming of cell fate through engineered intracrine-, paracrine-, and endocrine-like mechanisms, Biomaterials 32 (11) (2011) 3053–3061, https://doi.org/10.1016/j.biomaterials.2010.12.036.
[160] A. Geraili, M. Janmaleki, A. Sanati-Nezhad, K. Mequanint, Scalable microfabrication of drug-loaded core-shell tablets from a single erodible polymer with adjustable release profiles, Biofabrication 12 (4) (2020), 045007, https://doi.org/10.1088/1758-5090/ab97a0.
[161] X. Li, Y. Wei, K. Wen, Q. Han, K. Ogino, G. Ma, Novel insights on the encapsulation mechanism of PLGA terminal groups on ropivacaine, Eur. J. Pharm. Biopharm. 160 (2021) 143–151, https://doi.org/10.1016/j.ejpb.2021.01.015.
[162] A.M. Haaparanta, E. Jarvinen, I.F. Cengiz, V. Ella, H.T. Kokkonen, I. Kiviranta, M. Kellomaki, Preparation and characterization of collagen/PLA, chitosan/PLA, and collagen/chitosan/PLA hybrid scaffolds for cartilage tissue engineering, J. Mater. Sci. Mater. Med. 25 (4) (2014) 1129–1136, https://doi.org/10.1007/s10856-013-5129-5.
[163] E. Vatansever, D. Arslan, D.S. Sarul, Y. Kahraman, M. Nofar, Effects of molecular weight and crystallizability of polylactide on the cellulose nanocrystal dispersion quality in their nanocomposites, Int. J. Biol. Macromol. 154 (2020) 276–290, https://doi.org/10.1016/j.ijbiomac.2020.03.115.
[164] C.M. da Luz, M.S. Boyles, P. Falagan-Lotsch, M.R. Pereira, H.R. Tutumi, E. de Oliveira Santos, N.B. Martins, M. Himly, A. Sommer, I. Foissner, A. Duschl, J.M. Granjeiro, P.E. Leite, Poly-lactic acid nanoparticles (PLA-NP) promote physiological modifications in lung epithelial cells and are internalized by clathrin-coated pits and lipid rafts, J. Nanobiotechnol. 15 (1) (2017) 11, https://doi.org/10.1186/s12951-016-0238-1.
[165] D. Shen, H. Qi, W. Lin, W. Zhang, D. Bian, X. Shi, L. Qin, G. Zhang, W. Fu, K. Dou, B. Xu, Z. Yin, J. Rao, M. Alwi, S. Wang, Y. Zheng, D. Zhang, R. Gao, PDLLA-Zn-nitrided Fe bioresorbable scaffold with 53-mum-thick metallic struts and tunable multistage biodegradation function, Sci. Adv. 7 (23) (2021), https://doi.org/10.1126/sciadv.abf0614.
[166] F.L. Nie, Y.F. Zheng, S.C. Wei, C. Hu, G. Yang, In vitro corrosion, cytotoxicity and hemocompatibility of bulk nanocrystalline pure iron, Biomed. Mater. 5 (6) (2010), 065015, https://doi.org/10.1088/1748-6041/5/6/065015.
[167] M. Moravej, F. Prima, M. Fiset, D. Mantovani, Electroformed iron as new biomaterial for degradable stents: development process and structure-properties relationship, Acta Biomater. 6 (5) (2010) 1726–1735, https://doi.org/10.1016/j.actbio.2010.01.010.
[168] T.C. Paim, D.P. Wermuth, I. Bertaco, C. Zanatelli, L.I.S. Naasani, M. Slaviero, D. Driemeier, L. Schaeffer, M.R. Wink, Evaluation of in vitro and in vivo biocompatibility of iron produced by powder metallurgy, Mater Sci Eng C Mater Biol Appl 115 (2020), 111129, https://doi.org/10.1016/j.msec.2020.111129.
[169] D.T. Chou, D. Wells, D. Hong, B. Lee, H. Kuhn, P.N. Kumta, Novel processing of iron-manganese alloy-based biomaterials by inkjet 3-D printing, Acta Biomater. 9 (10) (2013) 8593–8603, https://doi.org/10.1016/j.actbio.2013.04.016.
[170] M. Cisternas, H. Bhuyan, M.J. Retamal, N. Casanova-Morales, M. Favre, U.G. Volkmann, P. Saikia, D.E. Diaz-Droguett, S. Mandl, D. Manova, N. Moraga, A. Chandia-Cristi, A. Alvarez, F. Guzman, Study of nitrogen implantation in Ti surface using plasma immersion ion implantation & deposition technique as biocompatible substrate for artificial membranes, Mater Sci Eng C Mater Biol Appl 113 (2020), 111002, https://doi.org/10.1016/j.msec.2020.111002.
[171] M.F. Maitz, R.W. Poon, X.Y. Liu, M.T. Pham, P.K. Chu, Bioactivity of titanium following sodium plasma immersion ion implantation and deposition, Biomaterials 26 (27) (2005) 5465–5473, https://doi.org/10.1016/j.biomaterials.2005.02.006.
[172] M. Fromel, M. Li, C.W. Pester, Surface engineering with polymer brush photolithography, Macromol. Rapid Commun. 41 (18) (2020), e2000177, https://doi.org/10.1002/marc.202000177.
[173] J. Fu, Y. Su, Y.X. Qin, Y. Zheng, Y. Wang, D. Zhu, Evolution of metallic cardiovascular stent materials: a comparative study among stainless steel, magnesium and zinc, Biomaterials 230 (2020), 119641, https://doi.org/10.1016/j.biomaterials.2019.119641.
[174] D. Zhu, I. Cockerill, Y. Su, Z. Zhang, J. Fu, K.W. Lee, J. Ma, C. Okpokwasili, L. Tang, Y. Zheng, Y.X. Qin, Y. Wang, Mechanical strength, biodegradation, and in vitro and in vivo biocompatibility of Zn biomaterials, ACS Appl. Mater. Interfaces 11 (7) (2019) 6809–6819, https://doi.org/10.1021/acsami.8b20634.
[175] R.J. Guillory 2nd, M. Sikora-Jasinska, J.W. Drelich, J. Goldman, In vitro corrosion and in vivo response to zinc implants with electropolished and anodized surfaces, ACS Appl. Mater. Interfaces 11 (22) (2019) 19884–19893, https://doi.org/10.1021/acsami.9b05370.
[176] M. Sikora-Jasinska, E. Mostaed, A. Mostaed, R. Beanland, D. Mantovani, M. Vedani, Fabrication, mechanical properties and in vitro degradation behavior of newly developed ZnAg alloys for degradable implant applications, Mater Sci Eng C Mater Biol Appl 77 (2017) 1170–1181, https://doi.org/10.1016/j.msec.2017.04.023.
[177] J. Niu, Z. Tang, H. Huang, J. Pei, H. Zhang, G. Yuan, W. Ding, Research on a Zn-Cu alloy as a biodegradable material for potential vascular stents application, Mater

Sci Eng C Mater Biol Appl 69 (2016) 407–413, https://doi.org/10.1016/j.msec.2016.06.082.
[178] E. Mostaed, M. Sikora-Jasinska, M.S. Ardakani, A. Mostaed, I.M. Reaney, J. Goldman, J.W. Drelich, Towards revealing key factors in mechanical instability of bioabsorbable Zn-based alloys for intended vascular stenting, Acta Biomater. 105 (2020) 319–335, https://doi.org/10.1016/j.actbio.2020.01.028.
[179] V. Mihalache, C. Negrila, I. Mercioniu, N. Iacob, V. Kuncser, Zn-Fe-oxide nanostructures of different iron concentrations for multifunctional applications: properties and precursor influence, Phys. Chem. Chem. Phys. 23 (30) (2021) 16107–16127, https://doi.org/10.1039/d1cp01002f.
[180] V.Q. Do, Y.S. Seo, J.M. Park, J. Yu, M.T.H. Duong, J. Nakai, S.K. Kim, H.C. Ahn, M.Y. Lee, A mixture of chloromethylisothiazolinone and methylisothiazolinone impairs rat vascular smooth muscle by depleting thiols and thereby elevating cytosolic Zn(2+) and generating reactive oxygen species, Arch. Toxicol. 95 (2) (2021) 541–556, https://doi.org/10.1007/s00204-020-02930-z.
[181] C. Chen, R. Yue, J. Zhang, H. Huang, J. Niu, G. Yuan, Biodegradable Zn-1.5Cu-1.5Ag alloy with anti-aging ability and strain hardening behavior for cardiovascular stents, Mater Sci Eng C Mater Biol Appl 116 (2020), 111172, https://doi.org/10.1016/j.msec.2020.111172.
[182] C. Garcia-Mintegui, L.C. Cordoba, J. Buxadera-Palomero, A. Marquina, E. Jimenez-Pique, M.P. Ginebra, J.L. Cortina, M. Pegueroles, Zn-Mg and Zn-Cu alloys for stenting applications: from nanoscale mechanical characterization to in vitro degradation and biocompatibility, Bioact. Mater. 6 (12) (2021) 4430–4446, https://doi.org/10.1016/j.bioactmat.2021.04.015.
[183] S. Lin, X. Ran, X. Yan, W. Yan, Q. Wang, T. Yin, J.G. Zhou, T. Hu, G. Wang, Corrosion behavior and biocompatibility evaluation of a novel zinc-based alloy stent in rabbit carotid artery model, J. Biomed. Mater. Res. B Appl. Biomater. 107 (6) (2019) 1814–1823, https://doi.org/10.1002/jbm.b.34274.
[184] J. Wu, D. Zhao, B. Lee, A. Roy, R. Yao, S. Chen, Z. Dong, W.R. Heineman, P.N. Kumta, Effect of lithium and aluminum on the mechanical properties, in vivo and in vitro degradation, and toxicity of multiphase ultrahigh ductility Mg-Li-Al-Zn quaternary alloys for vascular stent application, ACS Biomater. Sci. Eng. 6 (4) (2020) 1950–1964, https://doi.org/10.1021/acsbiomaterials.9b01591.
[185] E. Farabi, J.A. Sharp, A. Vahid, D.M. Fabijanic, M.R. Barnett, S.C. Gallo, Development of high strength and ductile Zn-Al-Li alloys for potential use in bioresorbable medical devices, Mater Sci Eng C Mater Biol Appl 122 (2021), 111897, https://doi.org/10.1016/j.msec.2021.111897.
[186] P.K. Bowen, J.M. Seitz, R.J. Guillory 2nd, J.P. Braykovich, S. Zhao, J. Goldman, J.W. Drelich, Evaluation of wrought Zn-Al alloys (1, 3, and 5 wt % Al) through mechanical and in vivo testing for stent applications, J. Biomed. Mater. Res. B Appl. Biomater. 106 (1) (2018) 245–258, https://doi.org/10.1002/jbm.b.33850.
[187] H.A. Tran, P.A. Tran, In situ coatings of silver nanoparticles for biofilm treatment in implant-retention surgeries: antimicrobial activities in monoculture and coculture, ACS Appl. Mater. Interfaces 13 (35) (2021) 41435–41444, https://doi.org/10.1021/acsami.1c08239.
[188] M. Shimabukuro, Antibacterial property and biocompatibility of silver, copper, and zinc in titanium dioxide layers incorporated by one-step micro-arc oxidation: a review, Antibiotics (Basel). 9 (10) (2020), https://doi.org/10.3390/antibiotics9100716.
[189] M. Watroba, W. Bednarczyk, J. Kawalko, P. Bala, Fine-tuning of mechanical properties in a Zn-Ag-Mg alloy via cold plastic deformation process and post-deformation annealing, Bioact. Mater. 6 (10) (2021) 3424–3436, https://doi.org/10.1016/j.bioactmat.2021.03.017.
[190] C. Hehrlein, B. Schorch, N. Kress, A. Arab, C. von Zur Muhlen, C. Bode, T. Epting, J. Haberstroh, L. Mey, H. Schwarzbach, R. Kinscherf, V. Stachniss, S. Schiestel, A. Kovacs, H. Fischer, E. Nennig, Zn-alloy provides a novel platform for mechanically stable bioresorbable vascular stents, PLoS One 14 (1) (2019), e0209111, https://doi.org/10.1371/journal.pone.0209111.
[191] A.A. Oliver, M. Sikora-Jasinska, A.G. Demir, R.J. Guillory 2nd, Recent advances and directions in the development of bioresorbable metallic cardiovascular stents: insights from recent human and in vivo studies, Acta Biomater. 127 (2021) 1–23, https://doi.org/10.1016/j.actbio.2021.03.058.
[192] K. Takahata, Y.B. Gianchandani, K.D. Wise, Micromachined antenna stents and cuffs for monitoring intraluminal pressure and flow, J. Microelectromech. Syst. 15 (5) (2006) 1289–1298, https://doi.org/10.1109/Jmems.2006.880229.
[193] E.Y. Chow, Y. Ouyang, B. Beier, W.J. Chappell, P.P. Irazoqui, Evaluation of cardiovascular stents as antennas for implantable wireless applications, Ieee T Microw. Theory 57 (10) (2009) 2523–2532, https://doi.org/10.1109/Tmtt.2009.2029954.
[194] D. Son, J. Lee, D.J. Lee, R. Ghaffari, S. Yun, S.J. Kim, J.E. Lee, H.R. Cho, S. Yoon, S.X. Yang, S. Lee, S.T. Qiao, D.S. Ling, S. Shin, J.K. Song, J. Kim, T. Kim, H. Lee, J. Kim, M. Soh, N. Lee, C.S. Hwang, S. Nam, N.S. Lu, T. Hyeon, S.H. Choi, D.H. Kim, Bioresorbable electronic stent integrated with therapeutic nanoparticles for endovascular diseases, ACS Nano 9 (6) (2015) 5937–5946, https://doi.org/10.1021/acsnano.5b00651.
[195] A.J. Heeger, Semiconducting and metallic polymers: the fourth generation of polymeric materials, Synthetic Met. 125 (1) (2001) 23–42, https://doi.org/Doi 10.1016/S0379-6779(01)00509-4.
[196] L. Ding, C. Hang, S. Cheng, L. Jia, L. Mou, L. Tang, C. Zhang, Y. Xie, W. Zheng, Y. Zhang, X. Jiang, A soft, conductive external stent inhibits intimal hyperplasia in vein grafts by electroporation and mechanical restriction, ACS Nano (2020), https://doi.org/10.1021/acsnano.0c04827.
[197] H. Jinnouchi, S. Torii, A. Sakamoto, F.D. Kolodgie, R. Virmani, A.V. Finn, Fully bioresorbable vascular scaffolds: lessons learned and future directions, Nat. Rev. Cardiol. 16 (5) (2019) 286–304, https://doi.org/10.1038/s41569-018-0124-7.
[198] P. Libby, G.K. Hansson, Inflammation and immunity in diseases of the arterial tree: players and layers, Circ. Res. 116 (2) (2015) 307–311, https://doi.org/10.1161/CIRCRESAHA.116.301313.
[199] P. Chytrosz, M. Golda-Cepa, J. Wlodarczyk, J. Kuzdzal, M. El Fray, A. Kotarba, Characterization of partially covered self-expandable metallic stents for esophageal cancer treatment: in vivo degradation, ACS Biomater. Sci. Eng. 7 (4) (2021) 1403–1413, https://doi.org/10.1021/acsbiomaterials.0c01773.
[200] R. Diletti, H.M. Garcia-Garcia, R.J. van Geuns, V. Farooq, L. Bailey, S. Rousselle, G. Kopia, W. Easterbrook, M. Pomeranz, P.W. Serruys, Angiographic and histological results following implantation of a novel stent-on-a-wire in the animal model, EuroIntervention 8 (3) (2012) 390–399, https://doi.org/10.4244/EIJV8I3A59.
[201] S. Chatterjee, K. Fujiwara, N.G. Perez, M. Ushio-Fukai, A.B. Fisher, Mechanosignaling in the vasculature: emerging concepts in sensing, transduction and physiological responses, Am. J. Physiol. Heart Circ. Physiol. 308 (12) (2015) H1451–H1462, https://doi.org/10.1152/ajpheart.00105.2015.
[202] D. Pierson, J. Edick, A. Tauscher, E. Pokorney, P. Bowen, J. Gelbaugh, J. Stinson, H. Getty, C.H. Lee, J. Drelich, J. Goldman, A simplified in vivo approach for evaluating the bioabsorbable behavior of candidate stent materials, J. Biomed. Mater. Res. B Appl. Biomater. 100 (1) (2012) 58–67, https://doi.org/10.1002/jbm.b.31922.
[203] A.A. Barros, C. Oliveira, A.J. Ribeiro, R. Autorino, R.L. Reis, A.R.C. Duarte, E. Lima, In vivo assessment of a novel biodegradable ureteral stent, World J. Urol. 36 (2) (2018) 277–283, https://doi.org/10.1007/s00345-017-2124-3.
[204] P.K. Bowen, J. Drelich, J. Goldman, Zinc exhibits ideal physiological corrosion behavior for bioabsorbable stents, Adv. Mater. 25 (18) (2013) 2577–2582, https://doi.org/10.1002/adma.201300226.
[205] V.V. Juettner, K. Kruse, A. Dan, V.H. Vu, Y. Khan, J. Le, D. Leckband, Y. Komarova, A.B. Malik, VE-PTP stabilizes VE-cadherin junctions and the endothelial barrier via a phosphatase-independent mechanism, J. Cell Biol. 218 (5) (2019) 1725–1742, https://doi.org/10.1083/jcb.201807210.
[206] C.M. Grimsley-Myers, R.H. Isaacson, C.M. Cadwell, J. Campos, M.S. Hernandes, K.R. Myers, T. Seo, W. Giang, K.K. Griendling, A.P. Kowalczyk, VE-cadherin endocytosis controls vascular integrity and patterning during development, J. Cell Biol. 219 (5) (2020), https://doi.org/10.1083/jcb.201909081.
[207] T. Heisler-Taylor, B. Kim, A.Y. Reese, S. Hamadmad, R. Kusibati, A.J. Fischer, C.M. Cebulla, A new multichannel method quantitating TUNEL in detached photoreceptor nuclei, Exp. Eye Res. 176 (2018) 121–129, https://doi.org/10.1016/j.exer.2018.06.028.
[208] R.J. Guillory 2nd, A.A. Oliver, E. Davis, E.J. Earley, J.W. Drelich, J. Goldman, Preclinical in-vivo evaluation and screening of zinc based degradable metals for endovascular stents, JOM (J. Occup. Med.) 71 (4) (2019) 1436–1446, https://doi.org/10.1007/s11837-019-03371-5, 1989.
[209] H. Tateishi, P. Suwannasom, Y. Sotomi, S. Nakatani, Y. Ishibashi, E. Tenekecioglu, M. Abdelghani, R. Cavalcante, Y. Zeng, M.J. Grundeken, F.N. Albuquerque, S. Veldhof, Y. Onuma, P.W. Serruys, A.C.B. s, Investigators of the, edge vascular response after resorption of the everolimus-eluting bioresorbable vascular scaffold- A 5-year serial optical coherence tomography study, Circ. J. 80 (5) (2016) 1131–1141, https://doi.org/10.1253/circj.CJ-15-1325.
[210] C. Indolfi, S. De Rosa, A. Colombo, Bioresorbable vascular scaffolds - basic concepts and clinical outcome, Nat. Rev. Cardiol. 13 (12) (2016) 719–729, https://doi.org/10.1038/nrcardio.2016.151.
[211] D. Dalos, C. Gangl, C. Roth, L. Krenn, S. Scherzer, M. Vertesich, I. Lang, G. Maurer, T. Neunteufl, R. Berger, G. Delle-Karth, Mechanical properties of the everolimus-eluting bioresorbable vascular scaffold compared to the metallic everolimus-eluting stent, BMC Cardiovasc. Disord. 16 (2016) 104, https://doi.org/10.1186/s12872-016-0296-1.
[212] S. De Rosa, C. Indolfi, Letter by De Rosa and Indolfi regarding article, "Clinical presentation and outcomes of coronary in-stent restenosis across 3-stent generations, Circ. Cardiovasc. Interv. 8 (4) (2015), https://doi.org/10.1161/CIRCINTERVENTIONS.115.002375.
[213] R.A. Byrne, G.W. Stone, J. Ormiston, A. Kastrati, Coronary balloon angioplasty, stents, and scaffolds, Lancet 390 (10096) (2017) 781–792, https://doi.org/10.1016/S0140-6736(17)31927-X.
[214] I. Cockerill, C.W. See, M.L. Young, Y. Wang, D. Zhu, Designing better cardiovascular stent materials - a learning curve, Adv. Funct. Mater. 31 (1) (2021), https://doi.org/10.1002/adfm.202005361.